

The Evolution of Temperature and Bolometric Luminosity in Type-II Supernovae

T. Faran,¹[★] E. Nakar,² and D. Poznanski²

¹*Racah Institute of Physics, The Hebrew University of Jerusalem, Jerusalem 91904, Israel*

²*School of Physics and Astronomy, Tel-Aviv University, Tel Aviv 69978, Israel.*

Accepted XXX. Received YYY; in original form ZZZ

ABSTRACT

In this work we present a uniform analysis of the temperature evolution and bolometric luminosity of a sample of 29 type-II supernovae (SNe), by fitting a black body model to their multi-band photometry. Our sample includes only SNe with high quality multi-band data and relatively well sampled time coverage. Most of the SNe in our sample were detected less than a week after explosion so their light curves cover the evolution both before and after recombination starts playing a role. We use this sample to study the signature of hydrogen recombination, which is expected to appear once the observed temperature drops to $\approx 7,000\text{K}$. Theory predicts that before recombination starts affecting the light curve, both the luminosity and the temperature should drop relatively fast, following a power-law in time. Once the recombination front reaches inner parts of the outflow, it sets the observed temperature to be nearly constant, and slows the decline of the luminosity (or even leads to a re-brightening). We compare our data to analytic studies and find strong evidence for the signature of recombination. We also find that the onset of the optical plateau in a given filter, is effectively the time at which the black body peak reaches the central wavelength of the filter, as it cools, and it does not correspond to the time at which recombination starts affecting the emission.

1 INTRODUCTION

Type II supernovae (SNe) are defined by the prominent hydrogen lines in their spectra. They are believed to originate from the collapse of an iron core of massive stars ($\gtrsim 8 M_{\odot}$) that retain their hydrogen envelope. The most common subtype, comprising ~ 70 percent of all type II SNe, is characterized by a phase of a roughly constant magnitude in the optical bands, hence their name type II-Plateau (II-P). This plateau phase typically starts 1–2 weeks after the explosion and lasts for ~ 100 d. Pre-explosion images have revealed that the progenitors of this class are red supergiants, in the mass range of $(7\text{--}16 M_{\odot})$ (Smartt 2015; for individual progenitor detections see e.g. Van Dyk et al. 2003a, Van Dyk et al. 2003b, Van Dyk et al. 2012). Type II-Linear (II-L) SNe constitutes another subclass of type II SNe (e.g., Patat et al. 1994; Arcavi et al. 2012; Faran et al. 2014a,b). They are spectroscopically very similar to type II-P events (Faran et al. 2014b, see), but their light curves are declining in all bands. In both types (II-P and II-L) there is typically a sharp drop in the luminosity after ~ 100 d and the luminosity starts to follow roughly the exponential decay expected from emission powered by the decay of ^{56}Ni . The distinction between these two classes is not well defined, and studies have used different definitions for II-L SNe. However, several recent works have shown that there exists a continuum of decline rates between slow declining and fast declining SNe (Ander-

son et al. 2014; Faran et al. 2014a), which suggests that a separation into two different classes may be artificial. Other type II sub-classes will not be discussed here. In this paper we focus on the light curves of type II-P and type II-L SNe, without making the distinction between the two types, and refer to them in short as type II SNe. Our goal here is to perform a uniform analysis of the bolometric luminosity and temperature evolution of a large sample of type II SNe and to compare our findings to theoretical models, focusing on the transition to the plateau, which takes place during the first two weeks.

There are several dozen type II SNe with detailed multi-wavelength observations. These are typically presented and analyzed individually (e.g., Leonard et al. 2002b; Maguire et al. 2010; Pastorello et al. 2009; Inserra et al. 2011; Takáts et al. 2014, 2015; Fraser et al. 2011; Tomasella et al. 2013; Dall’Ora et al. 2014; Barbarino et al. 2015; Valenti et al. 2015). There are only a few studies that analyze the bolometric properties and temperatures of a sample of type-II SNe. Bersten & Hamuy (2009) extracted bolometric light curves and effective temperature evolution for 33 SNe II-P, using calibrations for bolometric corrections from 3 well observed SNe. Valenti et al. (2016) derived the effective temperature from black body fits to photometric data of 30 type-II SNe, and calculated pseudo-bolometric light curves by integration over the optical bands. Lusk (2016) provides bolometric light curves and temperatures for 5 peculiar type II-P SNe that

originated from blue supergiants, by integrating over the observed photometry and correcting for the missing flux in the UV.

The theoretical interpretation of type II light curves is that the emission until the end of the plateau is dominated by the cooling emission, i.e., the leakage of radiation energy that was deposited in the envelope by the shock that unbinds it (Falk & Arnett 1977). Energy deposited by the decay of ^{56}Ni may contribute to this phase (e.g., Falk & Arnett 1977; Young 2004; Utrobin 2007), but this contribution is found to be subdominant (Nakar et al. 2016). The end of the plateau marks the release of all the internal energy deposited by the shock in the envelope. At later times the SN enters its nebular phase and the entire luminosity is driven by the decay of ^{56}Ni .

During the early stages of the light curve ($\sim 1-3$ weeks) the leakage of radiation is facilitated mostly by the drop in the optical depth of the outflow due to its expansion (Arnett 1980). Models predict that during this phase both the temperature and the bolometric luminosity drop roughly as power-laws in time (Nakar & Sari 2010; Rabinak & Waxman 2011; Shussman et al. 2016a). Once the observed temperature drop to ≈ 7000 K, hydrogen recombination becomes important and a recombination front starts moving from the outside towards inner parts of the ejecta. During this phase, recombination, rather than expansion, is the main driver of the drop in the optical depth of the outflow. As a result the observed temperature remains almost constant while the luminosity starts dropping much more slowly or even rises.

In this work we derive the temperatures and bolometric evolution of 29 type-II SNe with high quality multi-band light curves, by fitting a black body spectrum to their spectral energy distribution (SEDs). As will be discussed extensively below, these are far from trivial. SNe II are not blackbodies, and at different times several effects lead to systematic offsets from a pure black body in various bands. Nevertheless, guided by the data and theoretical insight, we derive the underlying black body properties. We compare the temporal evolution of the temperature and luminosity to theoretical predictions, paying special attention to signs of the recombination processes in the envelope. In Section 2 we describe the contents of our SN sample and the data, in Section 3 we explain how the black body fits to the data are done. Section A describes the results of the fitting and the possible effect of extinction on the results, and Section 5 presents a comparison of our results to theoretical expectations. We summarize our results in Section. 6.

2 THE SAMPLE

We construct from the literature a sample of 29 type-II SNe with good temporal coverage and multi-band photometry. The sample mostly relies on the SNe collected in Pejcha & Prieto (2015), Faran et al. (2014a) and (Faran et al. 2014b). The SNe in the sample were required to have sufficiently early data (starting less than 20 days after the explosion) and a well sampled light curves so the early behavior could be compared to the late behavior and to theoretical models. Some objects did not enter the sample despite having well sampled photometric curves, because their data was not good enough to produce good quality temperature and

luminosity curves. Ten of the objects have *Swift* UV observations, 10 have JHK data, and 7 objects have both JHK and UV. The photometric data were corrected for galactic extinction according to Cardelli et al. (1989), but not for host galactic extinction, since there is no method that can provide an accurate estimate for $E(B-V)_{\text{host}}$ (see for example the discussion in Faran et al. 2014a). We note however, that Faran et al. (2014a) found that $E(B-V)_{\text{host}}$ is typically small, of order 0.1 for nearby SNe. The explosion day is set as the mid-point between the first detection and the last non-detection of the SN, and the uncertainty is conservatively set as half the difference. Distance measurements were collected from NED¹ and averaged, using only distances based on the Tully-Fisher method, Cepheids, and SNe Ia. All of the objects are at low redshift with $z < 0.03$. The SN properties and their references are summarized in Table. 1.

3 BLACK BODY FITTING

We calculate the temperature and bolometric luminosity of the SNe at each epoch by fitting a black-body to the photometric data, according to $L_{\text{bol}} = 4\pi\sigma T^4 R^2$. We create a two-dimensional grid of temperatures evenly spaced by 20K, and black body radii (R) in the range of $10^{12}-10^{16}$ cm with spacing that corresponds to 0.002 mag. We then compute synthetic photometry from the black body distribution for every T and R values in each of the filter bands. Since data in different photometric bands were sometimes taken at different epochs, linear interpolation is used to account for the missing epochs. The interpolation is constrained to a maximum of 10 days from the nearest data point at early or late phases (before day 10 or after day 70), and to 20 days during intermediate phases, where the SN properties evolve more slowly.

A correct estimation of the photometric uncertainties is needed when fitting a black body to the photometry. Due to the relatively small number of data points, the fit is sensitive to errors that are under- or over-estimated. We therefore set a minimum value of 0.05 magnitudes to the error (such that the error is the maximal value between the given photometric error and 0.05 mag), which is a typical value for the scatter in our light curves. We assign the effective wavelength of the filter transmission curve to each band, and fit the data to find the black body temperature and radius by minimizing χ^2 . The uncertainty on the temperature is found by marginalizing the likelihood over the radius and finding the upper and lower temperature where $\chi^2 = \chi^2_{\text{min}} + 1$. To find the uncertainty in the luminosity, we calculate L_{bol} for every T and R , and find the contour in which $\chi^2 = \chi^2_{\text{min}} + 1$. The maximal and minimal values of L_{bol} are taken to be the upper and lower errors, respectively.

The SN spectrum is expected to follow a black body shape only in a limited frequency range, where $h\nu \sim kT$. At high frequencies the flux is suppressed by line blanketing, and at much lower frequencies, in the Rayleigh-Jeans (RJ) regime, it is predicted to be brighter than the RJ tail due

¹ The NASA/IPAC Extragalactic Database (NED) is operated by the Jet Propulsion Laboratory, California Institute of Technology, under contract with the National Aeronautics and Space Administration (NASA).

Table 1. SN Sample Details

SN name	Bands	Explosion day (MJD)	μ	z_{host}	Reference
SN1999em	U,B,V,R,I,J,H,K	51476 \pm 4	29.84 \pm 0.05	0.002	Leonard et al. (2002a) Pejcha & Prieto (2015)
SN1999gi	B,V,R,I	51519 \pm 4	30.24 \pm 0.04	0.002	Faran et al. (2014a)
SN2000dc	B,V,R,I	51762 \pm 4	32.93 \pm 0.14	0.010	Faran et al. (2014a)
SN2001cm	B,V,I	52064 \pm 1	33.18 \pm 0.10	0.011	Faran et al. (2014a)
SN2001cy	B,V,R,I	52086 \pm 6	33.01 \pm 0.12	0.015	Faran et al. (2014b)
SN2001do	B,V,R,I	52134 \pm 2	32.35 \pm 0.15	0.010	Faran et al. (2014b)
SN2001fa	B,V,R,I	52198 \pm 3	34.24 \pm 3.42	0.017	Faran et al. (2014b)
SN2001x	B,V,R,I	51963 \pm 5	31.59 \pm 0.11	0.005	Faran et al. (2014a)
SN2002gd	B,V,R,I	52553 \pm 15	32.90 \pm 0.21	0.009	Faran et al. (2014a)
SN2003hf	B,V,R,I	52864 \pm 2	35.51 \pm 3.55	0.031	Faran et al. (2014b)
SN2003hk	B,V,R,I	52860 \pm 2	34.41 \pm 0.20	0.023	Faran et al. (2014b)
SN2003iq	B,V,R,I	52920 \pm 2	32.28 \pm 0.08	0.008	Faran et al. (2014a)
SN2003z	B,V,R,I	52665 \pm 5	31.23 \pm 3.12	0.004	Faran et al. (2014a)
SN2004A	B,V,R,I	53007 \pm 7	31.61 \pm 0.32	0.003	Gurugubelli et al. (2008) Maguire et al. (2010)
SN2004du	B,V,R,I	53228 \pm 2	33.94 \pm 0.13	0.017	Faran et al. (2014a)
SN2004et	U,B,V,R,I,J,H,K	53271 \pm 1	28.41 \pm 0.07	0.000	Maguire et al. (2010)
SN2005cs	Swift UVOT,U,B,V,R,I,J,H,K	53549 \pm 0	29.36 \pm 0.01	0.002	Pastorello et al. (2009)
SN2006bp	Swift UVOT,U,B,V,r,i	53834 \pm 1	31.11 \pm 0.05	0.004	Quimby et al. (2007)
SN2007od	Swift UVOT,U,B,V,R,I,J,H,K	54399 \pm 8	32.29 \pm 0.17	0.006	Inserra et al. (2011)
SN2008in	Swift UVOT,U,B,V,R,I,J,H	54822 \pm 10	30.52 \pm 0.09	0.005	Roy & Kumar (2012)
SN2009N	Swift UVOT,B,g,V,R,r,I,i,J,H	54845 \pm 11	31.68 \pm 0.08	0.003	Takáts et al. (2014)
SN2009bw	Swift UV,U,B,V,R,I,J,H,K	54917 \pm 3	30.60 \pm 0.02	0.004	Inserra et al. (2012)
SN2009ib	U,u,B,g,V,R,r,I,i,J,H	55041 \pm 10	31.48 \pm 0.31	0.004	Takáts et al. (2015)
SN2012A	Swift UVOT,U,B,g,V,R,r,I,i,J,H,K	55929 \pm 5	29.72 \pm 0.17	0.003	Tomasella et al. (2013)
SN2012aw	Swift UVOT,U,u,B,g,V,R,r,I,i,J,H,K	56002 \pm 1	29.89 \pm 0.07	0.003	Bose et al. (2013) Dall'Orta et al. (2014)
SN2012ec	u,B,g,V,R,i,J,H,K	56143 \pm 10	31.57 \pm 0.45	0.005	Barbarino et al. (2015)
SN2013ab	Swift UVOT,U,B,g,V,R,r,I,i	56340 \pm 1	31.71 \pm 0.66	0.005	Bose et al. (2015a)
SN2013by	Swift UV,u,B,g,V,r,i	56407 \pm 11	30.84 \pm 0.15	0.004	Valenti et al. (2015)
SN2013ej	Swift UV *,U,u,B,g,V,R,r,I,i	56497 \pm 1	29.77 \pm 2.98	0.002	Richmond (2014) Valenti et al. (2014)

to the fact that the thermalization depth in this range is frequency dependent (Shussman et al. 2016a). We observe both effects in our data, and fit a black body only to the wavelength regions where it provides a good approximation.

In agreement with the theoretical predictions, we see that at high temperatures JHK observations cannot be well described by a standard black body spectrum, and tend to systematically lie above the RJ tail. This effect was recently modeled analytically by Shussman et al. (2016a) and will be further discussed in section 5.3. In the cases where this discrepancy is observed, we use only UV and optical data, and exclude the JHK bands.

As the temperature drops below $\sim 10,000 - 12,000$ K, line blanketing by iron group elements becomes strong and creates a deficiency in the measured UV flux, compared to a pure black body. The main species responsible for the strong absorption are Fe III and Ti III (Kasen & Woosley 2009). Line opacity is highly sensitive to the temperature, and even a slight cooling of the photosphere induces a fast recombination of Fe III and Ti III to Fe II and Ti II (Kasen & Woosley 2009; Eastman et al. 1996). The flux absorption becomes stronger and shifts further to the optical bands as the temperature continues to decrease to $\sim 8,000$ K. Figure 1 demonstrates the effect of line blanketing on the SED of SN2012aw on day 41. Data taken at wavelengths shorter than ~ 5000 were found to be affected by line blanketing and

were excluded from the fit (grey points), and only bands with wavelengths longer than 5000 were used (red points). The resulting black body at a temperature of 6420 K fits the red points very well and is also in very good agreement with a spectrum taken at the same epoch. The observed spectrum also confirms the flux cut-off around the *B*-band. In order to determine the time where the flux in each photometric band is suppressed by line-blanketing, we run the black body fitting procedure on each of the following filter groups: UV-UBVRIJHK, UBVRIJHK, BVRIJHK, VRIJHK and RIJHK, i.e., each time excluding the bluest band. We first determine, as an example, when the flux in the UV bands falls below the black body curve by looking at the fit to the UBVRIJHK regime. As long as the temperature is high enough, the UV flux will appear above the black body fit to UBVRIJHK or right on it. However, as the temperature decreases enough such that line blanketing starts to have an effect on the UV flux, the UV data points will drop below the UBVRIJHK curve. We exclude a certain band from the fit when it is $1-\sigma$ below the black body curve. This means that until that epoch we can use the UV-UBVRIJHK bands to determine the black body parameters, and from that day on we can only use the UBVRIJHK bands to fit the data. This procedure is repeated with the other bands to determine when the U, B, and V bands are affected by line blanketing and need to be excluded. The transition days co-

incide with the intersection between the temperature curves calculated with the bluest band, and the one calculated without it. Eventually, we construct the final temperature and luminosity curves using the transitions determined for each of the objects.

At early phases, when the temperature is higher than 10^4 K, the peak of F_λ occurs at wavelengths shorter than 3000 and UV observations are therefore crucial to constrain the fit parameters. JHK observations lie far from the peak of F_λ even at low temperatures (~ 6000 K), and therefore do not play a critical role in constraining the temperature. However, due to the exclusion of many of the bluer bands by line blanketing, it is necessary to have more data points in the red to improve the fit, meaning that JHK data become important at late epochs.

In order to quantify the importance of UV and Infra-Red (IR) photometry, we run a simulation and estimate the expected errors on the temperature in the absence of UV and IR. We produce synthetic photometry from black body distributions at temperatures 5000K–25,000K in 1000K bins, simulating a spread in the data using the typical photometric errors in each band. We then fit the synthetic data to a black body, repeating the process 100 times per temperature bin. The mean value and standard deviation (STD) of the best-fitting temperatures are computed, where we treat the STD as a measure of the typical statistical error. The uncertainties deduced from the simulation are presented as a function of the temperature in Figure. 2. From the upper panel of Figure. 2 one can see that at temperatures of $\sim 20,000$ K, the uncertainties on the temperature are quite high (over 800K) even with UV data. This reflects the fact that F_λ peaks at ~ 1300 , while the effective wavelength of the bluest filter we use (*Swift*–*uvw2*) is only at 2230. Below $T=15,000$ K, fits that do not include UV (but do include U) are able to reproduce the temperature with an accuracy of ~ 500 K. When *U*-band data is excluded, the fit reaches that accuracy below $T=12,000$ K.

At lower temperatures, corresponding to late epochs, most of the flux at wavelengths shorter than the B band is already affected by line blanketing and only bands with effective wavelengths longer than the V band can be used. In the bottom panel of Figure 2 it is evident that JHK data are important at $T > 7000$ K if the B band is not included, as the STD of the fit temperature is relatively high and rises rapidly with the model temperature. Although fitting with the V, R and I bands is still able to produce errors below 10%, we will see in Section 4.1 that the flux in the V band is typically absorbed by iron blanketing at ~ 6000 K. In the absence of JHK observations, we are left with only 3 data points for many objects - V, R and I. In these cases, it is impossible to determine when the V band falls below the black body curve, since we cannot examine the fit done without V, having only 2 data points at longer wavelengths. As a result, when an object does not have JHK data we typically cannot trust the temperature curve below ~ 6000 K and we do not fit the data below this temperature.

Throughout this paper, we consider only objects with U or UV data to deduce physical parameters at high temperatures (above $\sim 10,000$ K), and objects with JHK data at low temperatures (below ~ 6000 K).

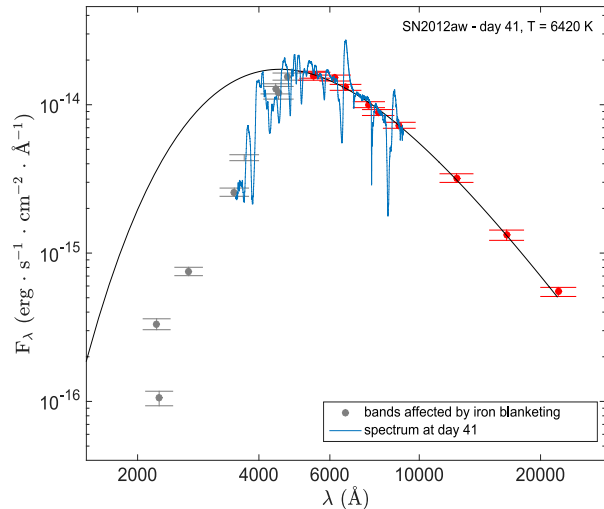


Figure 1. Black body fit of SN2012aw on day 41. The grey points represent bands that are affected by iron-blanketing and were therefore excluded from the fit. The black body curve fits the data very well above 5000, whereas at shorter wavelengths the SED is no longer represented by a black body. A spectrum taken on day 41 (Bose et al. 2013) is also shown to coincide well with the data, and confirms the flux cutoff around the *B*-band.

4 RESULTS

4.1 Temperature

The temperature curves are computed from the black body fits at each epoch and are presented in Figure. 3 (a list of all the results is also available in Appendix. A). After the explosion, the envelope expands and cools adiabatically. The typical temperatures during the first 10 days are above 10,000 degrees. In cases where UV data exist, the typical errors for that temperature range are smaller than ~ 500 K, and are comparable to the errors predicted by our simulations (see Section 3). Between 20 and 40 days after the explosion, the temperature curves start evolving more slowly compared to early phases. The flattening typically happens between 6000K and 7000K, and is therefore consistent with being associated with a recombination wave that propagates into the envelope and dictates the black body temperature to be the temperature of hydrogen recombination. This effect is analyzed and discussed in Section 5.2. We note that objects without JHK data do not show this flattening, since as discussed in Section 3, for these SNe we were not able to determine the time where the V-band can no longer be used and the fit stops when the temperature reaches 6000K.

As in Valenti et al. (2016), we observe that excluding UV data from the fit systematically leads to lower temperatures. This is true also for U, B and V, where the temperature produced without the bluest band is lower than that produced with it, before its flux is affected by iron blanketing. Since we do not observe this behavior in the simulation described in Section 3, the effect is not statistical and points to a deviation of the spectrum from a black body. We suggest that this is related to the re-distribution of energy that is absorbed by line blanketing. Most of the absorbed

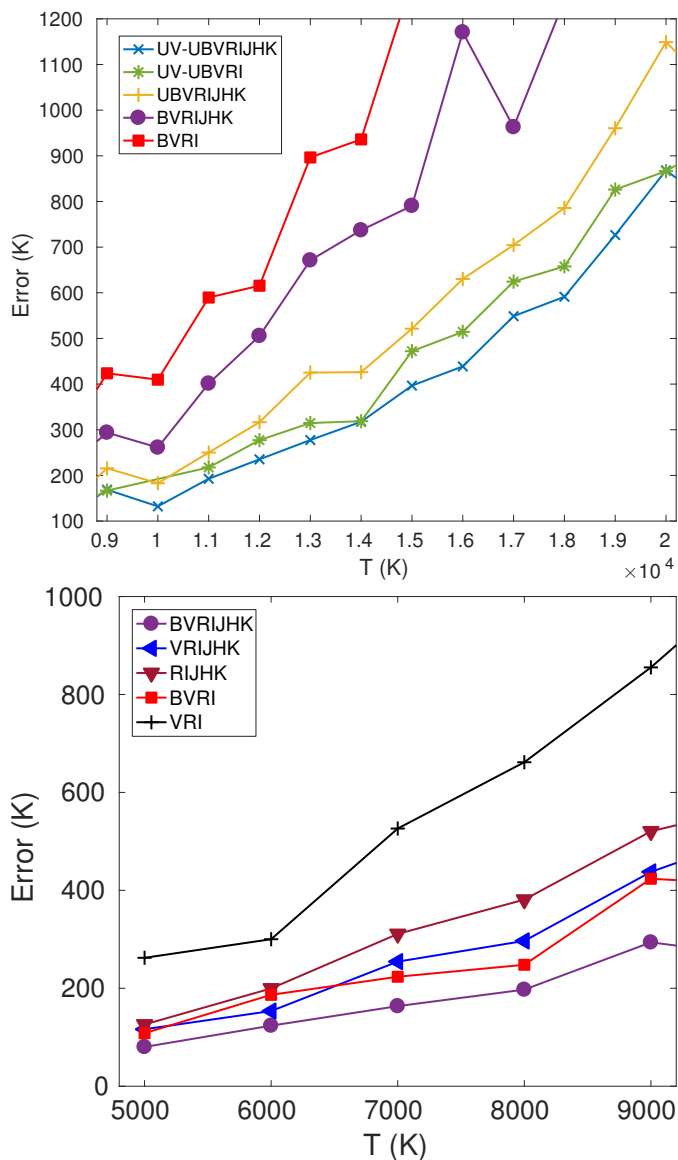


Figure 2. The expected uncertainties of the temperature of a black body, resulting from a simulation of synthetic data. The estimated uncertainties decrease as a function of the proximity of the bands to the black body peak, and therefore rise with the temperature.

radiation is expected to be re-emitted close to the absorption wavelength (see [Pinto & Eastman 2000](#)). As a result, the flux of the bluest band we use will be higher than the black body at the same temperature. Since the bands near the peak of the spectrum have the highest effect on the fit, that will result in higher fit temperatures. We redo the fits without the bluest band, and measure the flux under the resulting black body curve. We then measure the flux excess in the bands that lie above the black body curve, and the flux deficiency (due to line blanketing) in the bands below the black body curve and find that they are of the same order. This reinforces the assumption that the absorbed radiation by iron group elements is emitted at wavelengths close to the black body peak, and may add an uncertainty

to the temperature and bolometric luminosity that we measure. Above 10,000K, the temperatures calculated with the bluest band are $\approx 10\%$ higher than the ones calculated when it is omitted, and the difference becomes less significant at lower temperatures. The effect on the luminosity is higher and can get up to $\approx 10 - 20\%$. Therefore, the temperatures and bolometric luminosities presented in this paper can be overestimated by up to $\approx 10 - 20\%$.

We record the temperatures at which the flux in different bands starts being affected by line blanketing, and find that the typical temperature for UV is $\sim 11,000\text{K}$, and $\sim 8000\text{K}$ in the U and B bands. The V band seems to be affected around $\sim 6000\text{K}$. These results agree with the temperatures shown in [Eastman et al. \(1996\)](#)'s Figure. 7.

[Bersten & Hamuy \(2009\)](#) fit a black body to the photometry of SN1999em corrected to $A_V^{\text{host}} = 0.18$ and present its temperature and bolometric luminosity curves. After correcting our data to $A_V^{\text{host}} = 0.18$, we extract the temperature curve and compare it to the middle panel in [Bersten & Hamuy \(2009\)](#)'s Figure. 8. We find a good agreement between the values of the temperature and its evolution. The temperature computed at the first epoch, ~ 5 days, is around $13,000\text{K}$ in both curves and decreases to show a "bump" around day 16. Eventually, both curves settle on a temperature of $\sim 6000\text{K}$ in the middle of the plateau. [Valenti et al. \(2016\)](#) also fit a black body to several SNe that are included in our sample, but unfortunately the values are not provided, and we cannot perform a quantitative comparison.

4.2 Luminosity

The bolometric luminosity for each of the SNe is computed from the fit and the curves are presented in Figure. 4. Similarly to the temperature, the luminosity typically decreases as a power law during early epochs. The luminosity in most of the objects relents from its fast decline and starts to decrease more moderately, where the flattening seems to coincide with the break in the temperature. There are 3 objects whose luminosity not only flattens but also starts to rise. This happens for SN2004A and SN2009N at day 30 after explosion, and for SN2005cs at day 23. The transition in luminosity happens quite sharply and occurs when the temperatures are 6000K , 5900K and 6900K for the 3 objects, respectively. The change in the evolution of the luminosity is probably also related to the recombination of the envelope. We will discuss this further in Section 5. At the end of the plateau, the bolometric luminosity falls sharply.

We compare our bolometric luminosity curves to pseudo-bolometric curves from the literature by correcting for the different assumed distances to the SNe, and shifting in time to match the assumed explosion day. While broadly speaking there is mostly agreement between our work and previous efforts, there are still some discrepancies. The comparison is presented in Figure. 5. Pseudo-bolometric luminosities that were not computed with UV nor JHK data, as done for SN2009bw, SN2008in, and SN2004A, can be underestimated by up to 30% .

4.3 The Effect of Extinction

Host interstellar or circumstellar dust can introduce extinction that is not corrected for in our data (see Section 2),

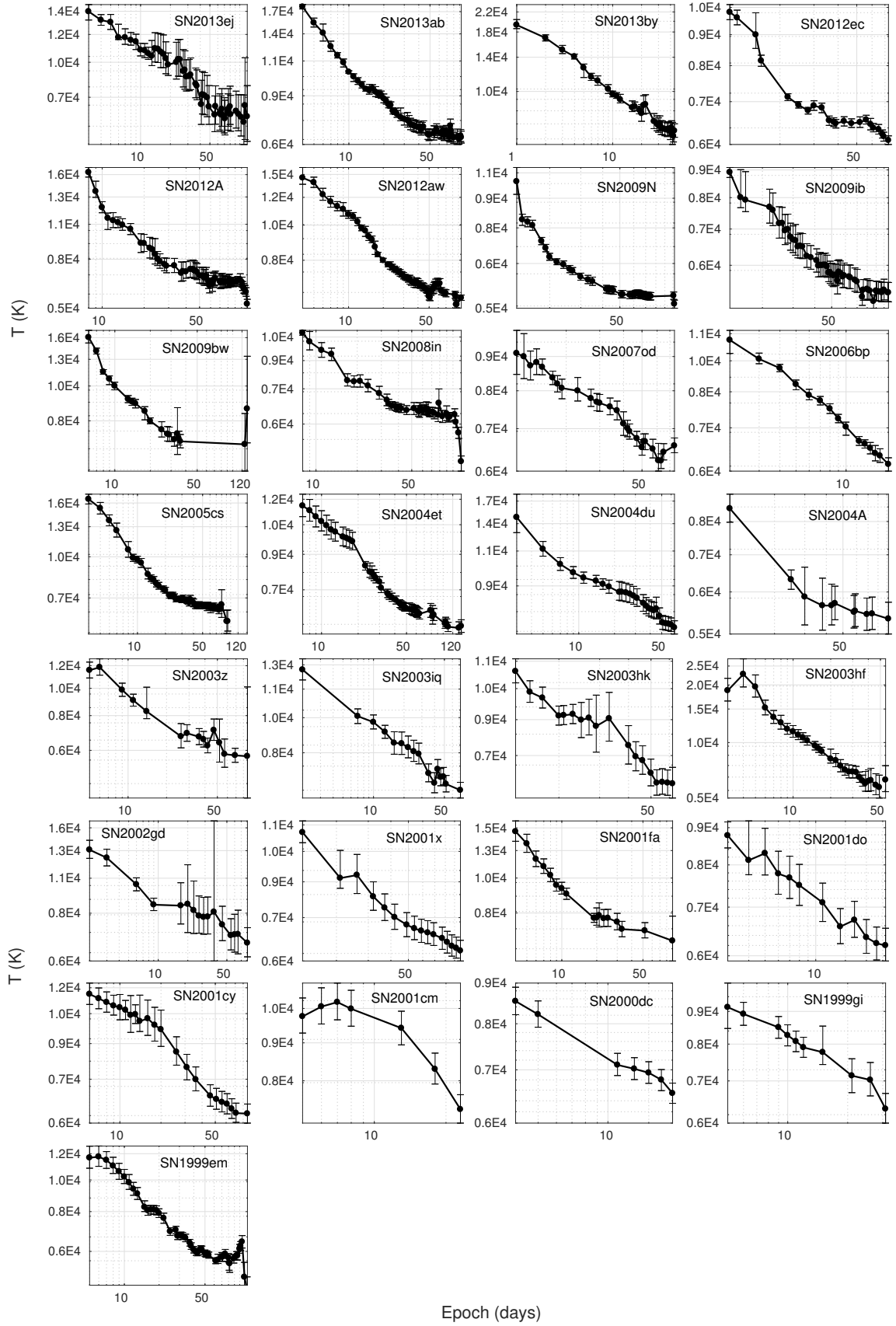


Figure 3. The temperature as a function of time for each SN in the sample.

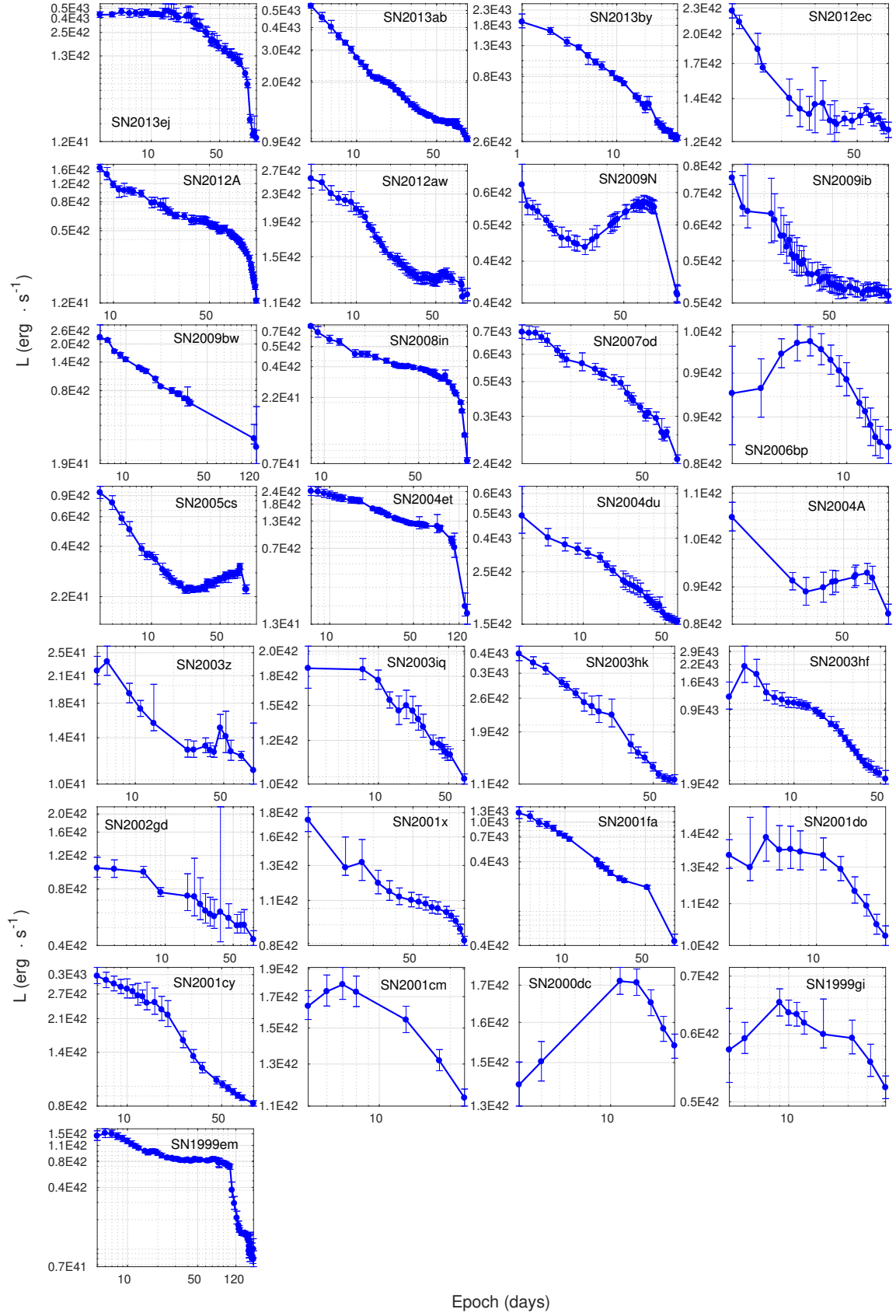


Figure 4. The bolometric luminosity curves as calculated from the black body fits for each SN in the sample.

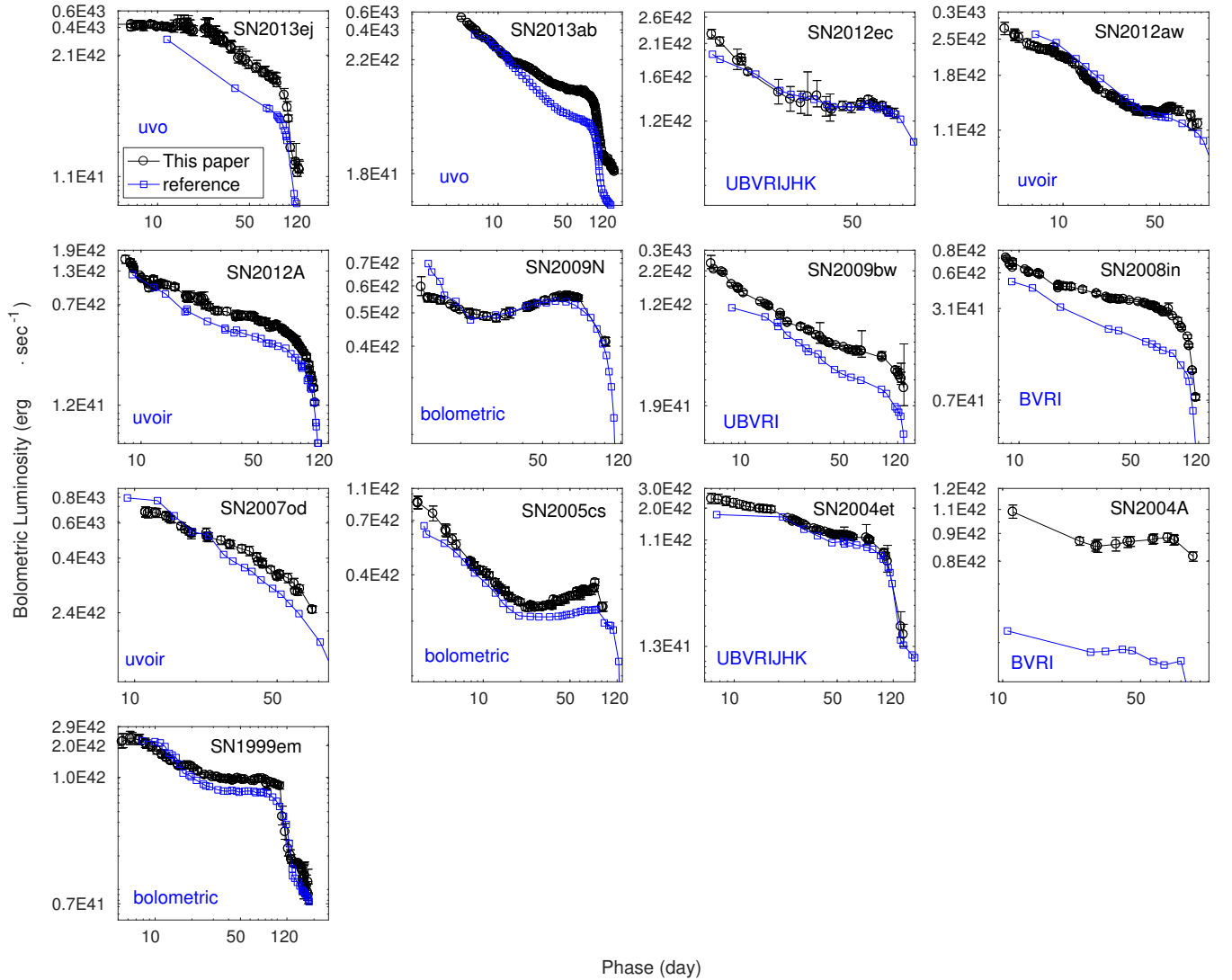


Figure 5. Comparison between the bolometric luminosity curves calculated in this paper (blue) and pseudo-bolometric curves from the literature (red), where the integrated wavelength range is specified. ‘*bolometric*’ light curves include bolometric corrections or are based on black body fits. Otherwise, the light curves are the integrated luminosity in the observed bands without any bolometric corrections. The luminosity of SN1999em presented here was calculated after correcting for $A_V^{\text{host}} = 0.18$, in order to compare to [Bersten & Hamuy \(2009\)](#). Discrepancies between the curves at early times are probably due to missing UV flux in the pseudo-bolometric curves. SN2012ec ([Barbarino et al. 2015](#)), SN2012aw ([Dall’Ora et al. 2014](#)), SN2012A ([Tomasella et al. 2013](#)), SN2013ab ([Bose et al. 2015a](#)), SN2009N (flux in RJ was approximated by RJ tail, no corrections in the blue) ([Takáts et al. 2014](#)), SN2009bw ([Inserra et al. 2012](#)), SN2008in ([Roy & Kumar 2012](#)), SN2005cs (bolometric corrections) ([Pastorello et al. 2009](#)), SN2004et ([Maguire et al. 2010](#)), SN2004A ([Hendry et al. 2006](#); [Maguire et al. 2010](#)), SN1999em ([Bersten & Hamuy 2009](#)), SN2007od ([Inserra et al. 2011](#)), SN2013ej ([Bose et al. 2015b](#))

resulting in an underestimation of the fit temperatures and luminosities. Although it is quite difficult to find a good estimation for A_V^{host} , it is possible to quantify the effect a certain A_V value has on the fit parameters as a function of the temperature. We repeat the fitting procedure two more times assuming $E(B-V) = 0.1$ and 0.05 , and $R_V = 3.1$, using the galactic extinction laws of [Cardelli et al. \(1989\)](#). As most type-II SNe in our sample are expected to have $E(B-V)^{\text{host}} < 0.1$ ([Faran et al. 2014a](#)), this value is effectively an upper limit on the possible required corrections.

In Figure 6 we present the relation between the best fit temperatures resulting from the correction to $E(B-V)^{\text{host}} = 0.1$ ($A_V^{\text{host}} \approx 0.3$) and $E(B-V)^{\text{host}} = 0.05$ ($A_V^{\text{host}} \approx 0.1$) as a

function of the uncorrected SN temperatures. The dependence of the corrected temperatures on $T(A_V^{\text{host}} = 0)$ can be well described by a third order polynomial, according to the following relations:

$$T(A_V = 0.3) \approx 3.17T_3^3 - 587T_3^2 + 1630T_3 - 1730 \quad (1)$$

and:

$$T(A_V = 0.15) \approx 0.69T_3^3 - 9.14 \times 10^{-2}T_3^2 + 1150T_3 - 424, \quad (2)$$

where $T_3 \equiv T(A_V = 0)/10^3$. These relations offer a convenient way to estimate the error on a fit temperature, in the typical extinction range of $A_V^{\text{host}} = 0 - 0.3$ mag.

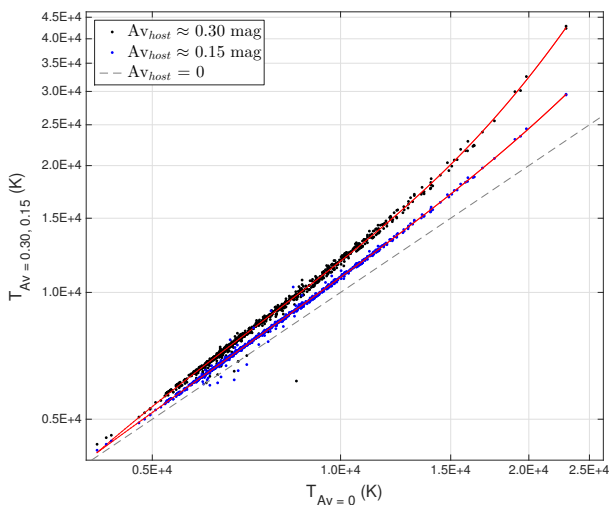


Figure 6. The best fit temperatures resulting from an extinction correction of $A_V^{\text{host}} = 0.3$ (black dots) and $A_V^{\text{host}} = 0.15$ (blue dots), as a function of $T(A_V^{\text{host}} = 0)$. The grey dashed line indicates $T = T_{A_V^{\text{host}}=0}$. The third order polynomial fits to the data are plotted in red and can be used to translate between the uncorrected and corrected temperatures.

Since the effect of extinction on the RJ is weak, we expect the luminosity to behave as $\frac{L_{AV}}{L_0} = \left(\frac{T_{AV}}{T_0}\right)^3$ at high temperatures. We fit the data with $T(A_V = 0) > 8000\text{K}$ according to this relation for both $A_V=0.3$ and $A_V=0.15$ and present the data and the fit in Figure 7. This, together with the previous relation for the temperatures, allows also the bolometric luminosity to be corrected for extinction as the relation holds down to low temperatures of $\sim 8000\text{K}$. Below that temperature, the corrections to L are less than 10%, which is of the order of the uncertainty.

5 COMPARISON TO THEORY

5.1 The Temperature at the Beginning of the Plateau

The formation process of the plateau in Type-II SNe and the origin of its shape (i.e., its luminosity and temperature evolution) are not fully understood. The common wisdom states that the plateau is formed due to a recombination wave that propagates into the envelope in Lagrangian coordinates. The recombination front defines the photosphere and therefore also fixes its temperature to the temperature of hydrogen recombination in the envelope. According to this view, the plateau should start when $T \approx 7500\text{K}$. However, more detailed theoretical models show that the peak in each photometric band is observed slightly before the black body peak enters the observed band. This is why redder bands peak at later time. Recombination prevents the observed temperature from falling below $\sim 6000\text{K}$, which is the main reason that after the peak the luminosity in the optical and IR bands falls rather slowly, and creates what is referred to as the plateau. We therefore expect to find photospheric temperatures higher than 7500K when the plateau starts.

We define the plateau starting time, t_p , in a specific band to be the day at which the light curve changes by less

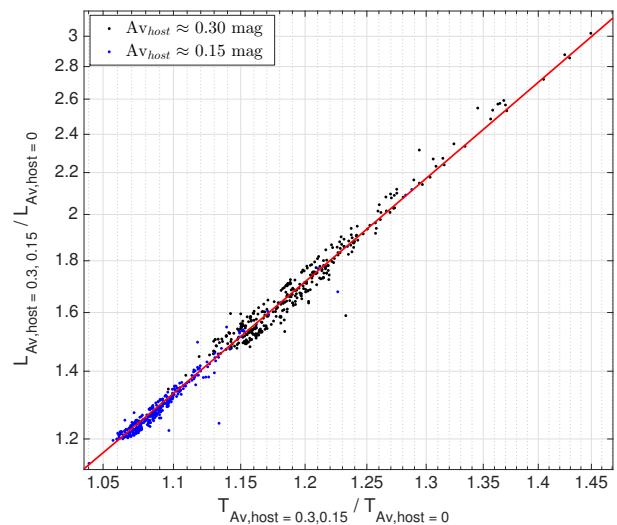


Figure 7. The ratio between the extinction corrected L_{bol} ($A_V^{\text{host}} = 0.3$ in black and $A_V^{\text{host}} = 0.15$ in blue) and the uncorrected L_{bol} , as a function of the similar temperature ratio for $T_{A_V^{\text{host}}=0} > 8000\text{K}$. Since extinction has a minimal effect on long wavelength observations, the Rayleigh-Jeans part of the spectrum at high temperatures is expected to be approximately fixed. Therefore, the data follow the relation: $\frac{L_{AV}}{L_0} = \left(\frac{T_{AV}}{T_0}\right)^3$, which is presented by the red line.

than 0.02 magnitudes per day. To find t_p , we fit a low order polynomial to the first 15-20 days and find the day where the derivative equals 0.02 mag/day. In order to estimate the uncertainties in t_p , we use the photometric errors of the data to generate random Gaussians errors, from which we create simulated data. We run the fit 1000 times on simulated data and use the mean of the results as the value of t_p and the standard deviation as its uncertainty. The value of t_p can be sensitive to the order of the polynomial and to the time range chosen for the fit. The maximal discrepancies introduced by changing those parameters are typically not larger than one day. We therefore set a minimal error of one day on t_p .

In Table 2 we present the t_p values computed in the R and I bands. Some objects have only an upper limit on t_p , since they were first observed already on the plateau. Nevertheless, for most of the objects it is clear that the plateau in R starts slightly before the plateau in I , as predicted by theory. In Figure 8 we demonstrate the different locations of the plateau in the R and in the I band for SN2012aw.

The temperatures associated with t_p in R and I are computed by interpolating the temperature curves to t_p . We plot the temperatures at t_p , i.e. $T_p = T(t = t_p)$ in the R -band for each SN in Figure 9. The blue arrows indicate the effect that $A_V^{\text{host}} = 0.3$ would have on T_p at $T \approx 8000\text{K}$ and $T \approx 11,000\text{K}$, according to equation 1. Objects with only lower limits (i.e., first data point lies already on the plateau) are presented by red triangles. Almost all T_p values lie above 8000K , and many of them above $10,000\text{K}$. The low luminosity SN2005cs shows an exceptionally high lower limit of $T_p \gtrsim 16,500\text{K}$. The observed range of T_p (with the exception of SN2005cs) is consistent with the theoretical light curves prediction by Shussman et al. (2016a). For example, the predicted R -band T_p for explosion energy of 10^{51} erg of progenitors with radii

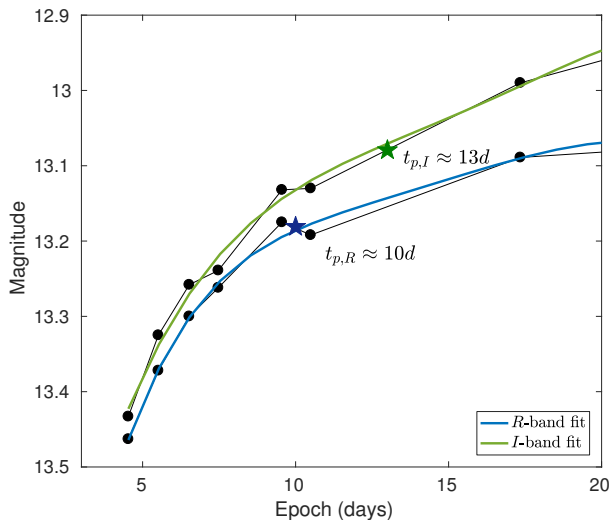


Figure 8. The locations of $t_{p,R}$ and $t_{p,I}$ of SN2012aw, as defined by the derivative of the polynomial fit to the R -band (blue) and the I -band (green). The plateau in the I -band appears to start slightly later than the plateau in the R -band.

in the range of $400 - 800 R_{\odot}$ and ejecta masses in the range of $7 - 15 M_{\odot}$ is between about 10,000K and 12,000K.

5.2 Signs of Recombination in the Temperature and Luminosity Curves

As discussed in Sections 4.1 and 4.2, the evolution of the temperature and the bolometric luminosity is characterized well by a power-law, that flattens when the temperature drops to $\sim 6000-7000$ K. We compute the early values of the logarithmic derivatives of the luminosity and temperature, α_L and α_T , respectively, during the first 15 days after the explosion. SNe that do not have U or UV data are excluded, since the temperatures at these epochs are typically higher than 12,000K, where U-band data (or bluer) are important to constrain the fit (see Section 3). We also calculate the late logarithmic derivatives between 40 and 100 days, while the SN light curve is on the plateau. For this we choose only SNe with IR data for the reasons discussed in Section 3. The results are summarized in Table 3. The best fit values for the early power law are highly sensitive to the exact value of the zero point in time. Since we make conservative explosion day estimates (see Section. 2), some of the uncertainties on the explosion day are as large as 5-10 days, and introduce non-negligible uncertainties to the values of the power law. The uncertainty values introduced from the fit itself and from the uncertainty on the explosion day are presented separately in Table 3. The values in the parentheses are the errors produced by the fit, and the upper and lower values are the differences from the α values that we get using the lower and upper boundaries of the explosion day estimate, respectively. In cases where the explosion day uncertainty is large (as in SN2013by, SN2012ec, SN2009jb and SN2008in) the upper and lower uncertainties are quite large. However, the explosion day uncertainty naturally has very little effect on the late values of α .

An example of the fit for α_T is shown in Figure. 10. It depicts the temperature curve of SN2005cs, on a loga-

rithmic scale. The best-fit logarithmic derivative computed during the first 15 days is $\alpha_T = -0.47 \pm 0.03$, and during days 40-100 is $\alpha_T = -0.06 \pm 0.07$. There is a clear flattening of the temperature curve between $t=19$ d and $t=35$ d, when the temperature is between 6500K and 7500K. In Figure 11 we present the temperature curves and the power law fits for all the objects that have both UV and IR data. From the values of the logarithmic derivatives (table 3) it is clear that at some point the temperature evolution flattens. At early time most values are in the range $\alpha_{T,early} \sim -0.6 - -0.2$ while at late time all best fit values are in the range $\alpha_{T,late} \sim -0.15 - 0$. The weighted mean values of the logarithmic derivatives are $\bar{\alpha}_{T,early} = -0.38 \pm 0.01$ and $\bar{\alpha}_{T,late} = -0.08 \pm 0.02$. Although it is not possible to point out the exact temperature of the transition, one can see that the range of temperatures between the two power law regimes is $\sim 6000-7000$ K, which is the temperature range expected from hydrogen recombination in type-II SN envelopes.

We also calculate the early and late logarithmic derivatives of L_{bol} . Similar to the temperature, the bolometric luminosity curves generally have a higher logarithmic derivative in the early phases. Most of the values of $\alpha_{L,early}$ are between -0.2 and -0.8, while most values of $\alpha_{L,late}$ are between -0.6 and 0.2, with weighted mean values of $\bar{\alpha}_{L,early} = -0.46 \pm 0.01$ and $\bar{\alpha}_{L,late} = -0.22 \pm 0.03$. When including the effect of extinction, we find that the values of $\alpha_{T,early}$ and $\alpha_{L,early}$ increase by ~ 0.1 and ~ 0.2 respectively, with an extinction value of $E(B - V) = 0.1$ mag. This result is also consistent with the expectation from recombination which is expected to cause a flatter, or even rising, light curves once the recombination front reaches facilitate the release of radiation from inner regions.

An interesting question is whether there are correlations between the early and late evolution, or between temperature and luminosity evolution. In Figure 12 we plot $\alpha_{T,late}$ vs. $\alpha_{T,early}$ (upper panel) and $\alpha_{L,late}$ vs. $\alpha_{L,early}$ (lower panel). The color coding refers to the decline rate of the V -band light curve per 100 days, calculated by linearly fitting the magnitude decline rate between day 25 and 75. The figures show no clear correlations between early and late evolution or between the late decline rate and the temperature evolution (early or late). However, there is a linear correlation between α_T and α_L .

Shussman et al. (2016a) provides theoretical predictions of $\alpha_{T,early}$ and $\alpha_{L,early}$ based on numerical simulations of SN explosions of a large set of RSG progenitors. They find that before recombination α_T is not strictly constant, and that it makes a transition from about -0.35 to -0.6. The time of steepening in α_T depends on the progenitor radius and ejecta velocity and for typical parameters it ranges between a day and two weeks. Since the data we have is not detailed enough to see the transition between the two power-laws, but only a single average power-law index, the analytic prediction is $\alpha_{T,early} \sim -0.35 - -0.6$. This range is marked in figure 12 and it is broadly consistent with the observed values listed in table 2. The theoretical model for the luminosity evolution predicts $\alpha_{L,early} \sim -0.35$. This value depends slightly on the progenitor radius (up to about ± 0.05) and more strongly on the progenitor structure (i.e., density profile). comparison of this prediction to the values listed in table 2 shows that they are consistent for most SNe but not for all. Moreover, the value of $\alpha_{L,early}$ is inconsistent with being similar to all

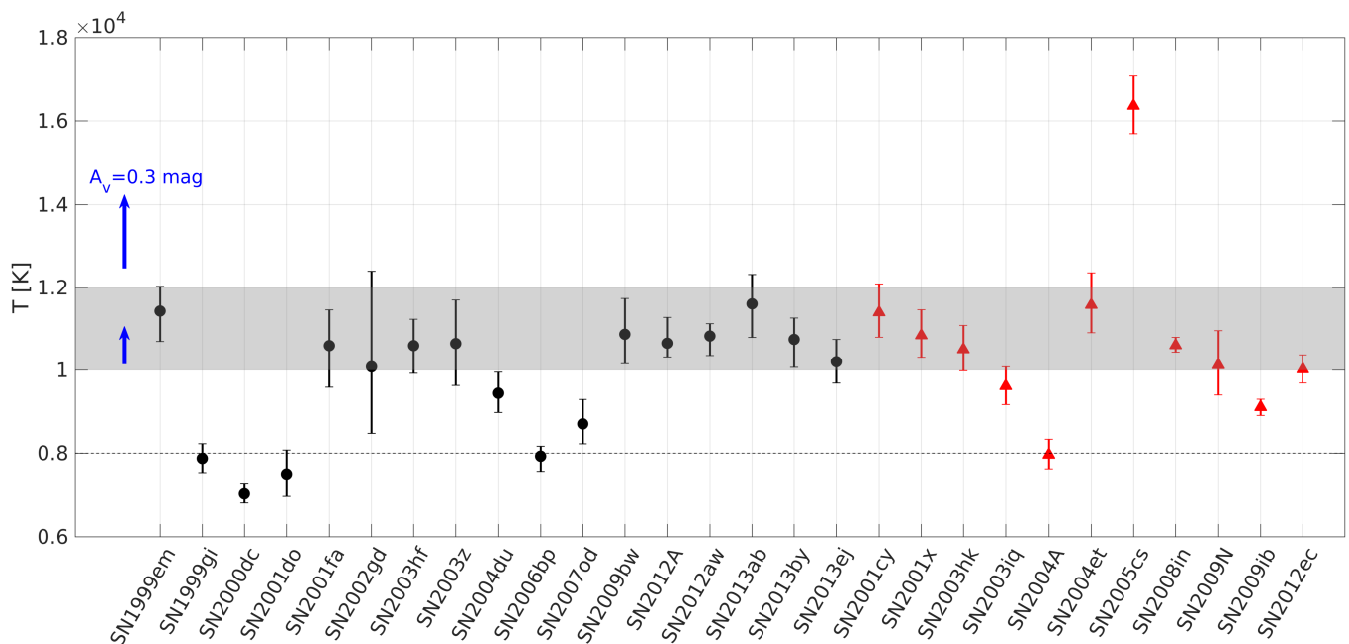


Figure 9. The temperatures at the onset of the plateau phase in the R band. Lower limits are marked by red triangles. The onset of the plateau is defined as the day in which the light curve changes by less than 0.02 magnitudes per day. Most of the temperatures lie above 8000K, which reinforced our claim that the flattening of the light curve is not caused by recombination. The blue arrows show the effect of extinction on T_p at $T \approx 11000\text{K}$ and $T \approx 8000\text{K}$ for $A_V = 0.3$. The plateau temperatures agree with radiative transfer results calculated by Shussman et al. (2016b) for a set of 124 RSGs, represented by the shaded area.

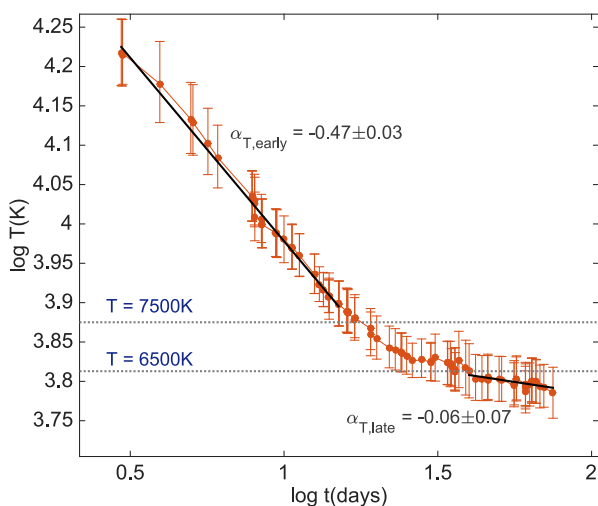


Figure 10. The temperature curve of SN2005cs on logarithmic scale. The temperature behaves as a broken power law, where in early phases it declines rapidly with a power of -0.47 ± 0.03 , and at late phases the power law is -0.06 ± 0.07 . This transition in the power law happens within the temperature range 6500–7500K, and we interpret it as the time when the color shell reaches the recombination temperature.

SNe. This is probably due to different density profiles of the progenitors.

5.3 Deviation from Black Body

At high temperatures, we find that a black body is not able to describe the whole observed spectrum not only at short wavelengths, where line blanketing is important, but also at long wavelengths on the RJ tail. In the left panel of Figure. 13 we show the SED of SN2012A on day 8, where the temperature is $\sim 15,000\text{K}$. The dashed blue line is the best fit to all of the data points, which clearly fails to fit the JHK observations. This effect is observed in all SNe that have early JHK data, which always seem to be brighter than the RJ tail at the temperature corresponding to the optical and UV flux.

Deviation of the RJ tail from a black body spectrum of early type II emission was seen in numerical simulations (e.g., Tominaga et al. 2011) and was modeled recently analytically by Shussman et al. (2016a). According to the model the reason for the deviation is that the flux at different wavelengths is determined at different locations in the outflow at different gas temperatures. Shussman et al. (2016a) find that on the RJ tail the modified spectrum can be approximated as $F_\nu \propto \nu^{1.4}$ and they also provide an approximation for the entire spectrum. The black solid line in the left panel of Figure. 13 is the best fit of Shussman et al. (2016a) model to the data of SN2012A. The model seems to fit the data very well throughout the UV and the IR and follows the JHK flux where it departs from a standard black body.

At lower temperatures both the standard black body model and the modified black body models are able to describe the JHK observations, as seen in the right panel of Figure. 13. The reason is that these bands are closer to the peak of the spectrum, where the models are essentially

SN name	t_p <i>R</i> -Band	T_p <i>R</i> -band	t_p <i>I</i> -Band	T_p <i>I</i> -band
SN1999em	8.0 (1.0)	11400^{+600}_{-800}	8.0 (1.1)	11400^{+700}_{-800}
SN1999gi	10.0 (1.0)	7900^{+400}_{-400}	10.0 (1.0)	7900^{+400}_{-400}
SN2000dc	13.0 (1.0)	7000^{+300}_{-300}	13.0 (1.0)	7000^{+300}_{-300}
SN2001cm			6.0*	9600^{+500*}_{-500}
SN2001cy	6.0*	11400^{+700*}_{-700}	6.0*	11400^{+700*}_{-700}
SN2001do	8.0 (1.0)	7500^{+600}_{-600}	11.0 (1.0)	7100^{+600}_{-500}
SN2001fa	8.0 (1.0)	10600^{+900}_{-1000}	9.0 (1.0)	10000^{+1000}_{-700}
SN2001x	13.0*	10800^{+700*}_{-600}	13.0*	10800^{+700*}_{-600}
SN2002gd	6.0 (3.0)	10000^{+2400}_{-1700}	6.0 (3.0)	10000^{+2400}_{-1700}
SN2003hf	13.0 (1.0)	10600^{+700}_{-700}	14.0 (1.1)	10400^{+700}_{-700}
SN2003hk	15.0*	10500^{+600*}_{-600}	16.0*	10500^{+600*}_{-600}
SN2003iq	7.0*	9600^{+500*}_{-500}	7.0*	9600^{+500*}_{-500}
SN2003z	9.0 (1.5)	11000^{+1100}_{-1100}	12.0 (1.6)	9300^{+700}_{-800}
SN2004A	11.0*	8000^{+400*}_{-400}	11.0*	8000^{+400*}_{-400}
SN2004du	10.0 (1.0)	9500^{+500}_{-500}	11.0 (1.0)	9300^{+500}_{-500}
SN2004et	9.0*	11600^{+800*}_{-700}	9.0*	11600^{+800*}_{-700}
SN2005cs	3.0*	16400^{+800*}_{-700}	3.0*	16400^{+800*}_{-700}
SN2006bp	8.0 (1.0)	7900^{+300}_{-400}	8.0 (1.0)	7900^{+300}_{-400}
SN2007od	9.0 (1.0)	8700^{+600}_{-600}	9.0 (1.0)	8700^{+600}_{-600}
SN2008in	9.0*	10600^{+200*}_{-200}	9.0*	10600^{+200*}_{-200}
SN2009N	14.0*	10100^{+900*}_{-800}	14.0*	10100^{+900*}_{-800}
SN2009bw	9.0 (1.0)	10900^{+900}_{-800}	11.0 (1.0)	9800^{+600}_{-600}
SN2009ib	13.0*	9100^{+200*}_{-300}	13.0*	9100^{+200*}_{-300}
SN2012A	13.0 (1.7)	10600^{+700}_{-400}	14.0 (1.0)	10400^{+600}_{-500}
SN2012aw	10.0 (1.1)	10800^{+300}_{-500}	13.0 (3.1)	10000^{+900}_{-1200}
SN2012ec	15.0*	10000^{+400*}_{-400}	15.0 *	10000^{+400*}_{-400}
SN2013ab	9.0 (1.0)	11600^{+800}_{-900}	9.0 (1.0)	11600^{+800}_{-900}
SN2013by	8.0 (1.0)	10700^{+600}_{-700}	8.0 (1.0)	10700^{+600}_{-700}
SN2013ej	12.0 (1.6)	10200^{+600}_{-600}	11.0 (1.4)	10400^{+600}_{-600}

Table 2. The times at which the *R*- and the *I*-bands enter the plateau phase, and the corresponding temperatures at those epochs.

equivalent. Also, at lower temperatures, where recombination starts affecting the spectrum the analytic model is no longer applicable.

6 SUMMARY

We calculated the temperatures and bolometric luminosities of 29 type-II SNe, by fitting black body models to their SEDs. We use the results to study the properties at the beginning of the plateau, to look for the signature of hydrogen recombination and to compare the observation before recombination becomes important to theoretical models. Our main findings are listed below.

- The temperature at the onset of the plateau phase in the *R*-band is above 8000K for all SNe in our sample, and exceeds 10,000K in many of them. This temperature changes as a function of the observed band, and is determined by the temperature at which the peak of the black body spectrum roughly coincides with the center of the filter transmission curve. This result is consistent with recent theoret-

ical models and is different than the common statement that the plateau phase starts once hydrogen recombinations becomes important. The temperatures we find agree with the predicted values for typical RSG progenitors of type-II SNe (Shussman et al. 2016a).

- We find that the temperature evolves with time as a power law, which flattens at $\sim 6000 - 8000$ K. We observe a similar evolution in the bolometric luminosity, where the logarithmic derivative at early phases is higher than that at late phases. The flattening is most likely a result of the recombination wave that exposes the inner layers. The values of the logarithmic derivatives for T and L_{bol} at early phases agree with predictions from simulations and analytic works (Shussman et al. 2016a; Nakar & Sari 2010).

- SN spectra deviate from a standard black body, both at low temperatures and short wavelengths due to line blanketing, and also at high temperatures and long wavelengths. We show that the SNe in our sample follow the analytic result from (Shussman et al. 2016a), that the flux on the RJ tail follows $F_{\nu} \propto \nu^{1.4}$.

SN name	$\alpha_{T,early}$	$\alpha_{T,late}$	$\alpha_{L,early}$	$\alpha_{L,late}$
SN1999em	-0.34 (0.06) $^{+0.18}_{-0.16}$	-0.05 (0.04) $^{+0.00}_{-0.00}$	-0.54 (0.09) $^{+0.28}_{-0.25}$	-0.06 (0.06) $^{+0.01}_{-0.01}$
SN2004et	-0.21 (0.12) $^{+0.01}_{-0.01}$	-0.11 (0.05) $^{+0.00}_{-0.00}$	-0.24 (0.17) $^{+0.01}_{-0.01}$	-0.24 (0.09) $^{+0.00}_{-0.00}$
SN2005cs	-0.47 (0.03) $^{+0.00}_{-0.00}$	-0.06 (0.07) $^{+0.00}_{-0.00}$	-0.68 (0.05) $^{+0.00}_{-0.00}$	0.13 (0.10) $^{+0.00}_{-0.00}$
SN2006bp	-0.27 (0.01) $^{+0.03}_{-0.03}$		-0.04 (0.01) $^{+0.01}_{-0.01}$	
SN2007od	-0.10 (0.27) $^{+0.06}_{-0.06}$	-0.09 (0.06) $^{+0.01}_{-0.01}$	-0.22 (0.29) $^{+0.14}_{-0.14}$	-0.81 (0.09) $^{+0.12}_{-0.12}$
SN2008in	-0.28 (0.10) $^{+0.28}_{-0.26}$	-0.07 (0.07) $^{+0.01}_{-0.01}$	-0.50 (0.12) $^{+0.49}_{-0.46}$	-0.52 (0.07) $^{+0.09}_{-0.09}$
SN2009N	-0.48 (0.22) $^{+0.35}_{-0.34}$	-0.07 (0.05) $^{+0.01}_{-0.01}$	-0.21 (0.19) $^{+0.15}_{-0.15}$	0.11 (0.05) $^{+0.02}_{-0.02}$
SN2009bw	-0.67 (0.05) $^{+0.23}_{-0.21}$	-0.04 (0.19) $^{+0.00}_{-0.00}$	-0.79 (0.07) $^{+0.25}_{-0.24}$	-0.29 (0.10) $^{+0.01}_{-0.01}$
SN2009ib	-0.29 (0.12) $^{+0.16}_{-0.15}$	-0.14 (0.08) $^{+0.02}_{-0.02}$	-0.32 (0.15) $^{+0.18}_{-0.17}$	-0.03 (0.05) $^{+0.00}_{-0.00}$
SN2012A	-0.84 (0.11) $^{+0.38}_{-0.37}$	-0.09 (0.06) $^{+0.01}_{-0.01}$	-1.07 (0.18) $^{+0.48}_{-0.47}$	-0.87 (0.07) $^{+0.06}_{-0.06}$
SN2012aw	-0.35 (0.02) $^{+0.02}_{-0.02}$	-0.11 (0.04) $^{+0.00}_{-0.00}$	-0.33 (0.03) $^{+0.02}_{-0.02}$	-0.09 (0.06) $^{+0.00}_{-0.00}$
SN2012ec	-0.50 (0.21) $^{+0.39}_{-0.38}$	-0.11 (0.07) $^{+0.02}_{-0.02}$	-0.75 (0.22) $^{+0.58}_{-0.56}$	-0.06 (0.13) $^{+0.01}_{-0.01}$
SN2013ab	-0.56 (0.02) $^{+0.07}_{-0.07}$		-0.80 (0.03) $^{+0.10}_{-0.10}$	
SN2013by	-0.30 (0.01) $^{+0.38}_{-0.84}$		-0.42 (0.01) $^{+0.49}_{-1.03}$	
SN2013ej	-0.21 (0.03) $^{+0.04}_{-0.03}$		-0.00 (0.05) $^{+0.00}_{-0.00}$	

Table 3. The early and late logarithmic derivatives of the temperature and the bolometric luminosity. The values of $\alpha_{T,early}$ and $\alpha_{L,early}$ increase by ≈ 0.1 and ≈ 0.2 respectively, with an extinction value of $E(B - V) = 0.1$ mag.

ACKNOWLEDGEMENTS

This research was supported by the I-Core center of excellence of the CHE-ISF. TF and EN were partially supported by an ERC starting grant (GRB/SN), an ISF grant (1277/13) and an ISA grant.

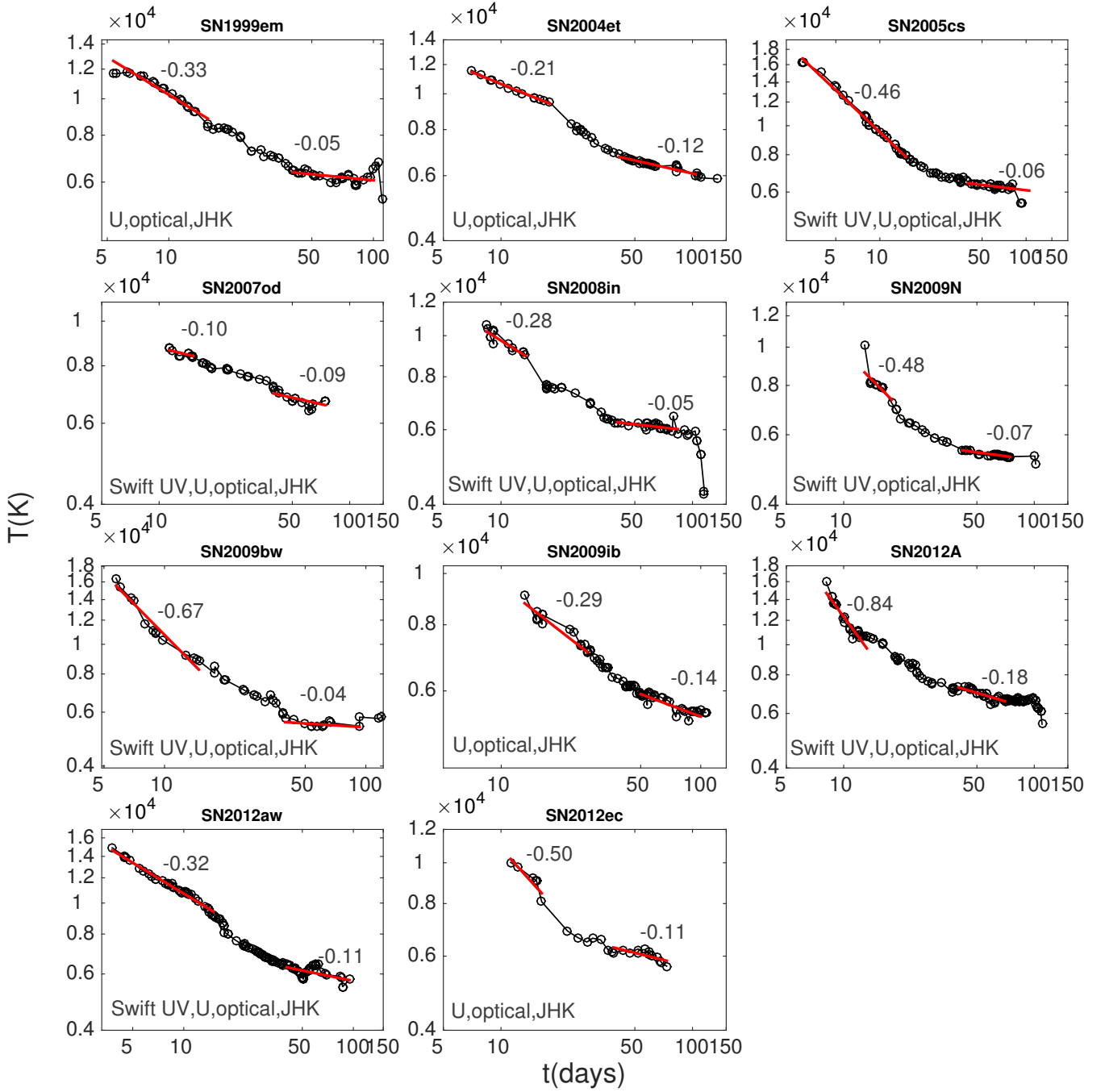


Figure 11. Temperature curves of objects that have both UV and JHK data. The numbers indicate the values of the best-fit early and late logarithmic derivative computed during the first 15 days, and during days 40-100 after the explosion, respectively. A clear flattening of the temperature is observed as the SN approaches the temperature of hydrogen recombination.

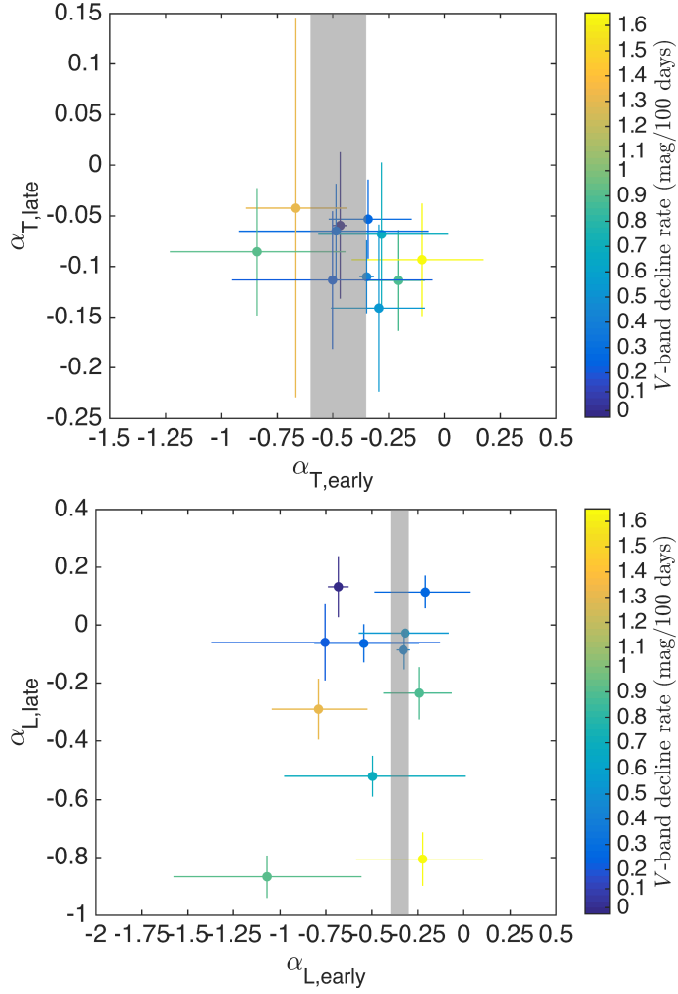


Figure 12. Top: the logarithmic derivative of the temperature at late times (40-100 days after the explosion) vs. the logarithmic derivative of the temperature at early times (up to 15 days after the explosion). The colors represent the decline rate of the V-band light curve. The values of the different objects agree with each other within the error-bars, and there is no apparent correlation with the light curve decline rate. Bottom: the same as the top figure for the bolometric luminosity. In this case, the early values of the logarithmic derivatives agree within the errors, but the late values show a wider spread. SNe whose luminosity declines faster at late phases (i.e., during the plateau phase) have faster declining light curves.

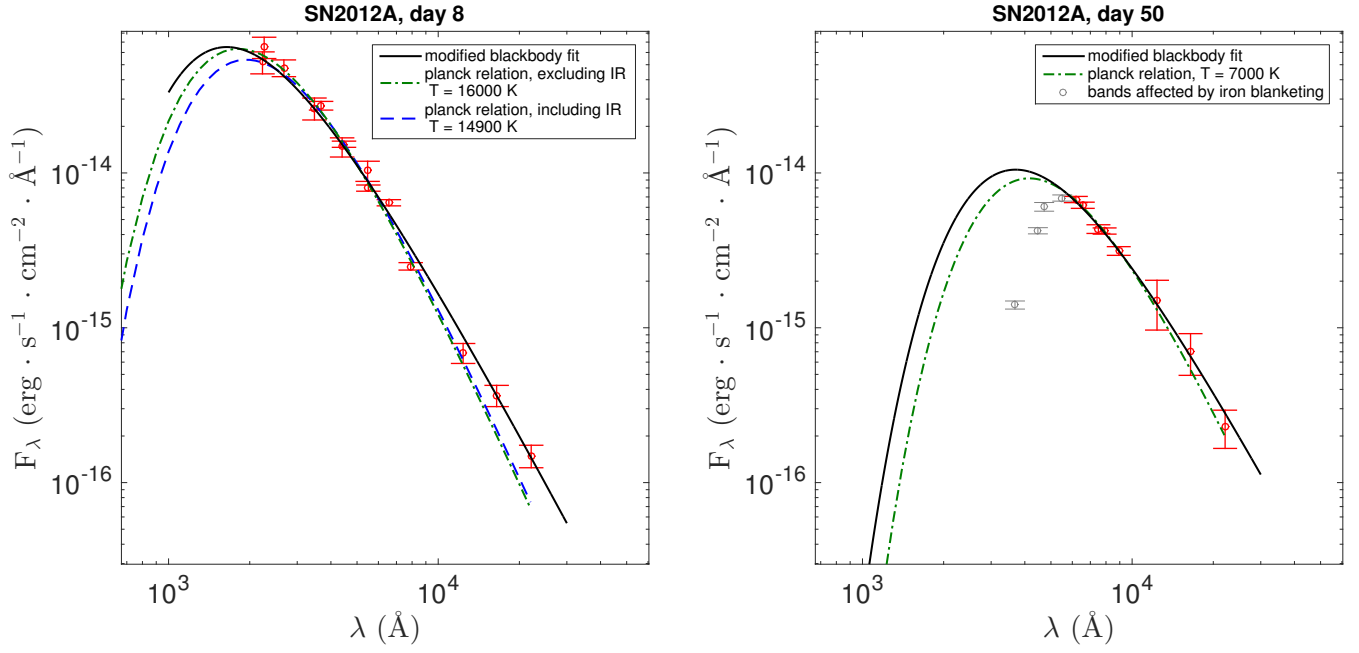


Figure 13. left: The SED of SN2012A at 8 days after the explosion. The standard Planck formula is only able to fit the peak of the distribution, but fails to fit the RJ tail. A modified black body model from Shussman et al. (2016a) is shown to be compatible throughout the whole wavelength range. right: An SED of SN2012A at 50 days past explosion. At this stage, after the onset of recombination and at low temperatures, both the modified black body and the standard model are able to describe the data.

REFERENCES

- Anderson J. P., et al., 2014, *ApJ*, **786**, 67
- Arcavi I., et al., 2012, *ApJ*, **756**, L30
- Arnett W. D., 1980, *ApJ*, **237**, 541
- Barbarino C., et al., 2015, *MNRAS*, **448**, 2312
- Bersten M. C., Hamuy M., 2009, *ApJ*, **701**, 200
- Bose S., et al., 2013, *MNRAS*, **433**, 1871
- Bose S., et al., 2015a, *MNRAS*, **450**, 2373
- Bose S., et al., 2015b, *ApJ*, **806**, 160
- Cardelli J. A., Clayton G. C., Mathis J. S., 1989, *ApJ*, **345**, 245
- Dall’Ora M., et al., 2014, *ApJ*, **787**, 139
- Eastman R. G., Schmidt B. P., Kirshner R., 1996, *ApJ*, **466**, 911
- Falk S. W., Arnett W. D., 1977, *ApJS*, **33**, 515
- Faran T., et al., 2014a, *MNRAS*, **442**, 844
- Faran T., et al., 2014b, *MNRAS*, **445**, 554
- Fraser M., et al., 2011, *MNRAS*, **417**, 1417
- Gurugubelli U. K., Sahu D. K., Anupama G. C., Chakradhari N. K., 2008, Bulletin of the Astronomical Society of India, **36**, 79
- Hendry M. A., et al., 2006, *MNRAS*, **369**, 1303
- Inserra C., et al., 2011, *MNRAS*, **417**, 261
- Inserra C., et al., 2012, *MNRAS*, **422**, 1122
- Kasen D., Woosley S. E., 2009, *ApJ*, **703**, 2205
- Leonard D. C., et al., 2002a, *PASP*, **114**, 35
- Leonard D. C., et al., 2002b, *AJ*, **124**, 2490
- Lusk J. A., 2016, SuperBoL: Module for calculating the bolometric luminosities of supernovae, Astrophysics Source Code Library (ascl:1609.019)
- Maguire K., et al., 2010, *MNRAS*, **404**, 981
- Nakar E., Sari R., 2010, *ApJ*, **725**, 904
- Nakar E., Poznanski D., Katz B., 2016, *ApJ*, **823**, 127
- Pastorello A., et al., 2009, *MNRAS*, **394**, 2266
- Patat F., Barbon R., Cappellaro E., Turatto M., 1994, *A&A*, **282**, 731
- Pejcha O., Prieto J. L., 2015, *ApJ*, **799**, 215
- Pinto P. A., Eastman R. G., 2000, *ApJ*, **530**, 757
- Quimby R. M., Wheeler J. C., Höflich P., Akerlof C. W., Brown P. J., Rykoff E. S., 2007, *ApJ*, **666**, 1093
- Rabinak I., Waxman E., 2011, *ApJ*, **728**, 63
- Richmond M. W., 2014, Journal of the American Association of Variable Star Observers (JAAVSO), **42**, 333
- Roy R., Kumar B., 2012, in Astronomical Society of India Conference Series. p. 115
- Shussman T., Waldman R., Nakar E., 2016a, preprint, ([arXiv:1610.05323](https://arxiv.org/abs/1610.05323))
- Shussman T., Nakar E., Waldman R., Katz B., 2016b, preprint, ([arXiv:1602.02774](https://arxiv.org/abs/1602.02774))
- Smartt S. J., 2015, *Publ. Astron. Soc. Australia*, **32**, e016
- Takáts K., et al., 2014, *MNRAS*, **438**, 368
- Takáts K., et al., 2015, *MNRAS*, **450**, 3137
- Tomasella L., et al., 2013, *MNRAS*, **434**, 1636
- Tominaga N., Morokuma T., Blinnikov S. I., Baklanov P., Sorokina E. I., Nomoto K., 2011, *ApJS*, **193**, 20
- Utrobin V. P., 2007, *A&A*, **461**, 233
- Valenti S., et al., 2014, *MNRAS*, **438**, L101
- Valenti S., et al., 2015, *MNRAS*, **448**, 2608
- Valenti S., et al., 2016, *MNRAS*, **459**, 3939
- Van Dyk S. D., Li W., Filippenko A. V., 2003a, *PASP*, **115**, 448
- Van Dyk S. D., Li W., Filippenko A. V., 2003b, *PASP*, **115**, 1289
- Van Dyk S. D., et al., 2012, *ApJ*, **756**, 131
- Young T. R., 2004, *ApJ*, **617**, 1233

APPENDIX A: A LIST OF THE TEMPERATURES AND BOLOMETRIC LUMINOSITIES

This paper has been typeset from a T_EX/L^AT_EX file prepared by the author.

Table A1. A List of the Temperatures and Bolometric Luminosities

MJD	$t - t_{\text{explosion}}$	T(K)	L($10^{42} \text{ erg} \cdot \text{s}^{-1}$)
SN1999em			
51481	5	11670_{761}^{904}	$1.43_{0.14}^{0.19}$
51482	6	11748_{707}^{841}	$1.53_{0.15}^{0.17}$
51483	7	11493_{597}^{652}	$1.50_{0.12}^{0.14}$
51484	8	11075_{532}^{632}	$1.42_{0.10}^{0.13}$
51485	9	10681_{529}^{576}	$1.35_{0.09}^{0.11}$
51486	10	10320_{441}^{506}	$1.27_{0.07}^{0.09}$
51487	11	9944_{432}^{527}	$1.19_{0.07}^{0.09}$
51488	12	9539_{381}^{415}	$1.13_{0.05}^{0.06}$
51489	13	9250_{336}^{379}	$1.08_{0.05}^{0.05}$
51491	15	8481_{236}^{356}	$1.00_{0.04}^{0.04}$
51492	16	8300_{251}^{272}	$0.97_{0.06}^{0.06}$
51493	17	8340_{220}^{253}	$0.99_{0.05}^{0.06}$
51494	18	8340_{237}^{234}	$1.00_{0.05}^{0.05}$
51495	19	8310_{239}^{245}	$0.99_{0.05}^{0.05}$
51496	20	8160_{228}^{231}	$0.96_{0.05}^{0.05}$
51498	22	7899_{255}^{260}	$0.90_{0.05}^{0.05}$
51501	25	7250_{181}^{176}	$0.86_{0.04}^{0.04}$
51504	28	7320_{178}^{174}	$0.85_{0.03}^{0.04}$
51505	29	7040_{161}^{162}	$0.83_{0.03}^{0.03}$
51507	31	7060_{162}^{162}	$0.83_{0.03}^{0.03}$
51508	32	7040_{158}^{165}	$0.83_{0.03}^{0.03}$
51510	34	6950_{166}^{173}	$0.81_{0.03}^{0.03}$
51513	37	6740_{144}^{149}	$0.80_{0.03}^{0.03}$
51514	38	6600_{141}^{138}	$0.81_{0.03}^{0.03}$
51516	40	6440_{131}^{137}	$0.82_{0.03}^{0.03}$
51518	42	6340_{131}^{124}	$0.80_{0.03}^{0.03}$
51519	43	6320_{124}^{130}	$0.80_{0.02}^{0.03}$
51520	44	6360_{120}^{139}	$0.80_{0.02}^{0.03}$
51522	46	6480_{132}^{136}	$0.82_{0.03}^{0.03}$
51523	47	6460_{132}^{135}	$0.83_{0.03}^{0.03}$
51526	50	6300_{121}^{132}	$0.82_{0.03}^{0.03}$
51527	51	6260_{124}^{125}	$0.81_{0.03}^{0.03}$
51528	52	6260_{113}^{138}	$0.81_{0.02}^{0.03}$
51530	54	6220_{119}^{126}	$0.81_{0.02}^{0.03}$
51538	62	6000_{112}^{115}	$0.80_{0.02}^{0.02}$
51541	65	6033_{137}^{224}	$0.80_{0.03}^{0.05}$
51546	70	6150_{168}^{179}	$0.83_{0.04}^{0.04}$
51547	71	6140_{165}^{172}	$0.83_{0.04}^{0.04}$
51551	75	6270_{172}^{187}	$0.83_{0.04}^{0.04}$
51556	80	6120_{161}^{165}	$0.81_{0.04}^{0.04}$
51557	81	5920_{277}^{312}	$0.76_{0.07}^{0.08}$

Table A1 – *continued* A List of the Temperatures and Bolometric Luminosities

51558	82	5891 ³⁴¹ ₃₂₄	0.76 ^{0.09} _{0.08}
51565	89	6080 ¹⁶⁶ ₁₆₉	0.77 ^{0.04} _{0.04}
51570	94	6200 ¹⁶⁴ ₁₇₂	0.76 ^{0.03} _{0.04}
51572	96	6200 ¹⁶⁵ ₁₇₁	0.74 ^{0.03} _{0.03}
51576	100	6480 ¹⁸⁸ ₁₈₃	0.72 ^{0.04} _{0.03}
51578	102	6600 ¹⁹³ ₁₉₃	0.71 ^{0.04} _{0.04}
51581	105	6780 ²⁸⁰ ₂₆₆	0.69 ^{0.04} _{0.04}
51586	110	5400 ⁵³⁸ ₄₄₉	0.40 ^{0.08} _{0.06}
51592	116	4960 ⁴⁴⁷ ₃₆₇	0.29 ^{0.05} _{0.04}
51599	123	4960 ⁴³⁵ ₃₇₆	0.21 ^{0.04} _{0.03}
51604	128	5500 ²⁹² ₂₄₇	0.17 ^{0.02} _{0.01}
51606	130	5620 ²³³ ₂₃₀	0.16 ^{0.01} _{0.01}
51607	131	5620 ¹⁶³ ₁₄₄	0.16 ^{0.01} _{0.01}
51613	137	5640 ¹⁵⁴ ₁₆₂	0.14 ^{0.01} _{0.01}
51614	138	5640 ¹⁶¹ ₁₃₅	0.14 ^{0.01} _{0.01}
51619	143	5760 ¹⁵⁶ ₁₄₂	0.14 ^{0.01} _{0.01}
51620	144	5760 ¹³⁹ ₁₄₇	0.14 ^{0.01} _{0.01}
51624	148	5920 ¹⁵¹ ₁₅₂	0.15 ^{0.01} _{0.01}
51627	151	5900 ¹⁵⁸ ₁₄₄	0.14 ^{0.01} _{0.01}
51629	153	5940 ¹⁵⁰ ₁₅₅	0.14 ^{0.01} _{0.01}
51634	158	5960 ¹⁵⁹ ₁₅₀	0.13 ^{0.01} _{0.01}
51637	161	5880 ¹⁵⁸ ₁₆₅	0.12 ^{0.01} _{0.01}
51638	162	5160 ⁵⁹⁷ ₄₅₄	0.10 ^{0.02} _{0.01}
51639	163	5460 ⁷⁰⁷ ₅₄₆	0.11 ^{0.03} _{0.02}
51640	164	5300 ⁶⁸⁰ ₅₁₆	0.10 ^{0.03} _{0.02}
51641	165	5024 ¹⁵⁴⁹ ₅₁₈	0.09 ^{0.06} _{0.01}
51642	166	5640 ⁷⁷⁴ ₆₀₂	0.11 ^{0.03} _{0.02}
51643	167	5880 ⁶⁷¹ ₅₃₁	0.11 ^{0.03} _{0.02}
51644	168	5920 ⁷⁵¹ ₅₆₁	0.12 ^{0.03} _{0.02}
51650	174	5580 ⁵⁹⁵ ₄₇₂	0.09 ^{0.02} _{0.01}
51653	177	5400 ⁵³⁴ ₄₅₀	0.08 ^{0.02} _{0.01}
51655	179	6080 ⁷²⁷ ₅₇₁	0.10 ^{0.03} _{0.02}
51656	180	5560 ⁵⁸⁰ ₄₇₅	0.08 ^{0.02} _{0.01}
SN1999gi			
51524	5	8680 ⁷⁵² ₆₁₁	0.57 ^{0.07} _{0.05}
51525	6	8480 ³⁴⁷ ₃₂₃	0.59 ^{0.03} _{0.02}
51528	9	8100 ³⁰⁷ ₂₉₈	0.65 ^{0.02} _{0.02}
51529	10	7880 ²⁹¹ ₂₈₀	0.63 ^{0.02} _{0.02}
51530	11	7720 ²⁷⁶ ₂₆₉	0.63 ^{0.02} _{0.02}
51531	12	7560 ²⁶⁹ ₂₅₃	0.62 ^{0.02} _{0.02}
51534	15	7436 ⁷⁰⁰ ₃₀₇	0.60 ^{0.06} _{0.02}
51540	21	6860 ⁴¹¹ ₃₈₉	0.59 ^{0.03} _{0.02}
51545	26	6760 ⁴¹⁹ ₃₆₀	0.56 ^{0.03} _{0.02}

Table A1 – *continued* A List of the Temperatures and Bolometric Luminosities

51550	31	6120 ³³⁴ ₂₉₂	0.52 ^{0.02} _{0.02}
51556	37	5920 ³⁰⁸ ₂₇₄	0.50 ^{0.01} _{0.01}
51577	58	5320 ²⁴³ ₂₁₉	0.50 ^{0.01} _{0.01}
51582	63	5260 ²³² ₂₁₉	0.49 ^{0.01} _{0.01}
51590	71	5080 ²²³ ₁₉₇	0.50 ^{0.02} _{0.02}
51614	95	5140 ²¹⁸ ₂₁₁	0.45 ^{0.02} _{0.01}
51619	100	4960 ²⁰⁰ ₁₉₈	0.45 ^{0.02} _{0.01}
51624	105	4880 ²⁰⁵ ₁₈₁	0.43 ^{0.02} _{0.01}
51629	110	4880 ²⁰⁰ ₁₈₅	0.40 ^{0.01} _{0.01}
51634	115	4700 ¹⁷⁸ ₁₇₇	0.36 ^{0.02} _{0.01}
51638	119	4580 ¹⁶⁷ ₁₆₉	0.31 ^{0.01} _{0.01}
51643	124	4220 ¹⁴⁵ ₁₃₉	0.25 ^{0.01} _{0.01}
51648	129	4060 ²¹¹ ₁₈₅	0.17 ^{0.02} _{0.01}
51653	134	3760 ¹¹⁶ ₁₁₀	0.13 ^{0.01} _{0.01}
51658	139	3300 ¹⁵⁵ ₁₄₂	0.17 ^{0.03} _{0.02}
51664	145	3640 ¹⁰⁴ ₁₀₇	0.11 ^{0.01} _{0.01}
51669	150	3620 ¹⁰¹ ₁₀₈	0.11 ^{0.01} _{0.01}
SN2000dc			
51766	4	8540 ³⁵³ ₃₂₇	1.39 ^{0.06} _{0.06}
51767	5	8220 ³²⁷ ₃₀₀	1.46 ^{0.06} _{0.05}
51773	11	7100 ²⁴³ ₂₁₅	1.70 ^{0.05} _{0.04}
51775	13	7020 ²³¹ ₂₁₄	1.69 ^{0.05} _{0.04}
51777	15	6940 ²²⁶ ₂₀₈	1.63 ^{0.04} _{0.04}
51779	17	6800 ²⁰⁶ ₂₁₀	1.55 ^{0.04} _{0.04}
51781	19	6540 ¹⁹⁶ ₁₈₇	1.50 ^{0.03} _{0.04}
SN2001cm			
52069	5	9580 ⁴⁹⁴ ₄₂₄	1.63 ^{0.11} _{0.09}
52070	6	9840 ⁵¹⁶ ₄₅₅	1.73 ^{0.12} _{0.10}
52071	7	9960 ⁵³¹ ₄₆₇	1.78 ^{0.13} _{0.10}
52072	8	9780 ⁵⁰⁷ ₄₅₁	1.73 ^{0.11} _{0.10}
52077	13	9280 ⁴³⁸ ₄₁₃	1.54 ^{0.09} _{0.08}
52082	18	8300 ³⁷⁰ ₃₂₉	1.31 ^{0.06} _{0.05}
52087	23	7440 ³⁰³ ₂₇₃	1.13 ^{0.04} _{0.04}
SN2001cy			
52092	6	11400 ⁶⁸⁷ ₆₀₅	3.32 ^{0.33} _{0.27}
52093	7	11140 ⁶³⁸ ₅₈₇	3.17 ^{0.29} _{0.24}
52094	8	10920 ⁶¹⁵ ₅₅₇	3.05 ^{0.27} _{0.22}
52095	9	10720 ⁶¹⁴ ₅₁₆	2.95 ^{0.26} _{0.20}
52096	10	10620 ⁷⁵⁹ ₆₆₈	2.89 ^{0.34} _{0.27}
52097	11	10480 ⁵⁴⁸ ₅₁₉	2.81 ^{0.22} _{0.19}
52098	12	10200 ¹¹¹⁵ ₈₈₆	2.68 ^{0.39} _{0.26}
52099	13	10240 ⁵³⁵ ₄₈₀	2.66 ^{0.20} _{0.17}

Table A1 – *continued* A List of the Temperatures and Bolometric Luminosities

52100	14	9878 ¹⁴⁶⁰ ₅₂₂	2.48 ^{0.63} _{0.18}
52102	16	10020 ¹⁰²⁸ ₈₅₃	2.49 ^{0.42} _{0.30}
52104	18	9680 ⁹⁵⁴ ₇₈₇	2.30 ^{0.36} _{0.26}
52106	20	9460 ¹⁰¹⁷ ₈₁₂	2.17 ^{0.37} _{0.25}
52112	26	8400 ⁶⁹⁹ ₅₆₈	1.65 ^{0.18} _{0.12}
52117	31	7740 ⁵⁵³ ₄₉₅	1.38 ^{0.11} _{0.09}
52122	36	7260 ⁵⁰⁰ ₄₂₂	1.22 ^{0.08} _{0.06}
52132	46	6660 ⁴⁰² ₃₅₆	1.06 ^{0.05} _{0.04}
52137	51	6540 ³⁸⁹ ₃₃₆	1.02 ^{0.04} _{0.03}
52142	56	6440 ³⁷⁹ ₃₂₂	0.98 ^{0.04} _{0.03}
52147	61	6380 ³⁵⁷ ₃₂₆	0.94 ^{0.04} _{0.03}
52152	66	6220 ³³⁸ ₃₀₉	0.90 ^{0.03} _{0.03}
52157	71	6080 ³²⁷ ₂₉₀	0.88 ^{0.03} _{0.03}
52162	76	5940 ³²³ ₂₇₃	0.87 ^{0.03} _{0.02}
52167	81	5980 ³²⁰ ₂₇₆	0.86 ^{0.03} _{0.02}
52172	86	6060 ³¹⁸ ₂₉₄	0.83 ^{0.03} _{0.02}
52177	91	5820 ²⁹¹ ₂₆₉	0.77 ^{0.02} _{0.02}
52182	96	5600 ²⁷⁶ ₂₄₂	0.71 ^{0.02} _{0.02}
SN2001do			
52137	3	8780 ³⁸⁵ ₃₃₉	1.34 ^{0.07} _{0.06}
52138	4	8117 ¹⁰⁷⁷ ₃₆₂	1.29 ^{0.22} _{0.05}
52139	5	8300 ⁶⁸² ₅₅₁	1.42 ^{0.15} _{0.10}
52140	6	7780 ⁵⁷⁴ ₄₉₀	1.36 ^{0.11} _{0.08}
52141	7	7680 ⁵⁴⁴ ₄₈₆	1.36 ^{0.10} _{0.08}
52142	8	7500 ⁵¹⁴ ₄₆₂	1.35 ^{0.09} _{0.08}
52145	11	7100 ⁴⁵² ₄₁₂	1.34 ^{0.08} _{0.06}
52148	14	6580 ³⁸⁷ ₃₄₅	1.28 ^{0.05} _{0.05}
52151	17	6720 ⁴⁰⁹ ₃₅₉	1.19 ^{0.06} _{0.04}
52154	20	6360 ³⁷⁰ ₃₁₂	1.14 ^{0.04} _{0.04}
52157	23	6240 ³³² ₃₁₈	1.07 ^{0.04} _{0.03}
52160	26	6200 ³⁴⁷ ₂₉₈	1.03 ^{0.03} _{0.03}
52163	29	5900 ³⁰³ ₂₇₄	0.99 ^{0.03} _{0.03}
52166	32	5600 ²⁷¹ ₂₄₅	0.93 ^{0.02} _{0.03}
52169	35	5640 ²⁷³ ₂₅₁	0.87 ^{0.02} _{0.02}
52172	38	5520 ²⁵⁸ ₂₄₁	0.81 ^{0.02} _{0.02}
52175	41	5340 ²³⁹ ₂₂₇	0.77 ^{0.02} _{0.02}
52181	47	5120 ²¹⁸ ₂₀₈	0.69 ^{0.02} _{0.02}
52184	50	5160 ²²⁸ ₂₀₆	0.67 ^{0.02} _{0.02}
52187	53	4860 ²¹⁰ ₁₇₄	0.65 ^{0.02} _{0.02}
52190	56	4940 ²⁰² ₁₉₂	0.60 ^{0.02} _{0.02}
52193	59	4960 ¹⁹⁷ ₂₀₀	0.58 ^{0.02} _{0.02}
52198	64	4760 ¹⁹⁹ ₁₆₈	0.57 ^{0.02} _{0.02}
52203	69	4000 ²⁵⁴ ₂₃₉	0.69 ^{0.10} _{0.08}

Table A1 – *continued* A List of the Temperatures and Bolometric Luminosities

SN2001fa			
52202	4	14820 ¹²⁶² ₁₀₇₃	12.54 ^{2.21} _{1.66}
52203	5	13500 ¹⁰¹¹ ₈₇₉	11.47 ^{1.65} _{1.29}
52204	6	11980 ⁷⁷⁴ ₆₇₁	9.75 ^{1.09} _{0.86}
52205	7	11320 ⁶⁸² ₅₉₁	9.22 ^{0.90} _{0.72}
52206	8	10580 ⁵⁸³ ₅₁₀	8.46 ^{0.70} _{0.56}
52207	9	9800 ⁴⁷⁹ ₄₄₁	7.38 ^{0.49} _{0.42}
52208	10	9560 ⁴⁵⁸ ₄₁₄	6.97 ^{0.44} _{0.37}
52209	11	9160 ⁴¹⁶ ₃₇₇	6.38 ^{0.35} _{0.31}
52217	19	7600 ²⁸³ ₂₄₆	3.72 ^{0.12} _{0.11}
52218	20	7613 ⁶⁰⁹ ₄₁₉	3.30 ^{0.28} _{0.17}
52219	21	7760 ⁷⁸⁸ ₆₆₂	3.20 ^{0.32} _{0.21}
52221	23	7580 ⁵⁴² ₄₆₁	2.98 ^{0.22} _{0.17}
52223	25	7600 ⁵³² ₄₇₄	2.67 ^{0.20} _{0.15}
52228	30	7380 ⁵⁰⁷ ₄₃₈	2.33 ^{0.16} _{0.12}
52231	33	6980 ⁴³² ₃₉₉	2.20 ^{0.12} _{0.10}
52250	52	6900 ⁴⁴⁰ ₃₇₆	1.85 ^{0.10} _{0.08}
52278	80	5960 ⁴⁷⁸ ₄₀₇	0.53 ^{0.03} _{0.02}
52283	85	5740 ¹⁰¹³ ₇₃₅	0.48 ^{0.05} _{0.04}
52288	90	6380 ¹³³⁷ ₉₂₀	0.46 ^{0.10} _{0.05}
52293	95	5200 ⁸¹¹ ₅₉₇	0.33 ^{0.02} _{0.02}
SN2001x			
51976	13	10840 ⁶²⁴ ₅₃₃	1.76 ^{0.16} _{0.12}
51984	21	8669 ¹²⁵⁹ ₄₁₉	1.30 ^{0.28} _{0.06}
51989	26	8800 ⁹³³ ₇₅₉	1.34 ^{0.21} _{0.15}
51995	32	7920 ⁵⁹⁴ ₅₁₂	1.17 ^{0.10} _{0.08}
52000	37	7500 ⁵²⁶ ₄₅₃	1.11 ^{0.08} _{0.06}
52005	42	7160 ⁴⁷³ ₄₁₁	1.08 ^{0.06} _{0.05}
52012	49	6900 ⁴²⁴ ₃₈₈	1.05 ^{0.05} _{0.04}
52017	54	6780 ⁴²¹ ₃₆₃	1.04 ^{0.05} _{0.04}
52022	59	6700 ³⁹² ₃₆₇	1.03 ^{0.05} _{0.04}
52027	64	6640 ⁴⁰² ₃₄₆	1.00 ^{0.05} _{0.04}
52032	69	6580 ³⁹² ₃₄₂	1.00 ^{0.04} _{0.03}
52040	77	6460 ³⁶³ ₃₃₈	0.97 ^{0.04} _{0.03}
52045	82	6340 ³⁴⁵ ₃₂₈	0.95 ^{0.03} _{0.03}
52050	87	6220 ³⁵⁰ ₃₀₀	0.92 ^{0.03} _{0.03}
52055	92	6160 ³⁴⁰ ₂₉₅	0.88 ^{0.03} _{0.03}
52060	97	6080 ³¹⁸ ₂₉₇	0.81 ^{0.02} _{0.02}
52068	105	5760 ²⁹⁵ ₂₅₅	0.66 ^{0.02} _{0.02}
52074	111	5400 ²⁴¹ ₂₃₅	0.50 ^{0.01} _{0.01}
52081	118	4980 ²⁰⁵ ₁₉₇	0.34 ^{0.01} _{0.01}
52089	126	4620 ¹⁸⁷ ₁₆₇	0.24 ^{0.01} _{0.01}
52096	133	4760 ²⁵³ ₂₂₂	0.20 ^{0.01} _{0.01}

Table A1 – *continued* A List of the Temperatures and Bolometric Luminosities

52103	140	4500 ¹⁶⁴ ₁₆₁	0.19 ^{0.01} _{0.01}
52110	147	4580 ¹⁷³ ₁₆₄	0.18 ^{0.01} _{0.01}
SN2002gd			
52555	2	13120 ⁹⁸⁵ ₈₂₆	1.04 ^{0.15} _{0.11}
52556	3	12340 ⁸³⁹ ₇₃₃	1.02 ^{0.12} _{0.10}
52559	6	10080 ⁵²² ₄₇₇	0.99 ^{0.07} _{0.06}
52562	9	8640 ⁴⁴¹ ₃₇₈	0.77 ^{0.05} _{0.04}
52570	17	8580 ¹⁶³³ ₁₁₁₈	0.74 ^{0.23} _{0.12}
52573	20	8680 ³⁰³⁰ ₁₆₈₈	0.73 ^{0.44} _{0.15}
52576	23	8280 ²⁰⁶⁷ ₁₃₃₉	0.67 ^{0.26} _{0.11}
52579	26	7940 ¹²⁹⁷ ₉₈₃	0.61 ^{0.15} _{0.09}
52582	29	7860 ¹²⁷⁶ ₉₅₇	0.59 ^{0.14} _{0.08}
52585	32	7880 ¹²⁸³ ₉₆₂	0.57 ^{0.13} _{0.08}
52590	37	8180 ⁸¹⁶² ₂₅₄₈	0.61 ^{1.60} _{0.19}
52598	45	7420 ¹¹²¹ ₈₄₆	0.56 ^{0.11} _{0.06}
52608	55	6840 ⁹²⁸ ₇₁₅	0.51 ^{0.08} _{0.04}
52613	60	6880 ¹¹⁵⁵ ₈₅₅	0.51 ^{0.09} _{0.05}
52618	65	6900 ¹³⁸⁸ ₉₅₅	0.52 ^{0.11} _{0.05}
52634	81	6460 ⁷⁹⁵ ₆₄₈	0.43 ^{0.05} _{0.03}
52659	106	5680 ¹¹⁶³ ₈₁₃	0.22 ^{0.03} _{0.01}
52664	111	5300 ¹⁸⁰⁰ ₁₀₄₁	0.15 ^{0.04} _{0.01}
SN2003hf			
52867	3	19000 ²⁸⁷³ ₂₁₆₅	11.39 ^{4.17} _{2.54}
52868	4	22940 ⁴⁴⁵⁴ ₃₁₄₂	21.50 ^{11.31} _{6.09}
52869	5	19820 ²⁹²⁶ ₂₂₀₅	18.27 ^{6.68} _{4.11}
52870	6	15560 ¹⁴⁴² ₁₂₁₅	12.45 ^{2.48} _{1.82}
52871	7	13960 ¹¹²¹ ₉₅₈	11.19 ^{1.78} _{1.36}
52872	8	13120 ¹¹⁵⁴ ₉₅₁	10.75 ^{1.73} _{1.25}
52873	9	12180 ⁸²⁶ ₇₀₅	10.13 ^{1.20} _{0.95}
52874	10	11820 ⁸⁵⁹ ₇₃₅	10.05 ^{1.21} _{0.93}
52875	11	11380 ⁷¹⁹ ₅₉₇	9.83 ^{1.02} _{0.78}
52876	12	11040 ⁶³⁹ ₅₈₃	9.61 ^{0.89} _{0.74}
52877	13	10660 ⁵⁹⁵ ₅₃₆	9.33 ^{0.79} _{0.66}
52879	15	10040 ⁵¹⁹ ₄₇₀	8.54 ^{0.62} _{0.52}
52880	16	9740 ⁴⁹⁴ ₄₃₃	8.13 ^{0.55} _{0.46}
52881	17	9420 ⁴⁵⁴ ₄₀₅	7.67 ^{0.47} _{0.40}
52884	20	8641 ¹⁰²⁵ ₄₁₅	6.51 ^{1.10} _{0.35}
52886	22	8480 ⁷⁰² ₅₉₄	6.14 ^{0.66} _{0.50}
52888	24	7960 ⁶⁰¹ ₅₂₂	5.41 ^{0.48} _{0.36}
52890	26	7620 ⁵⁵² ₄₆₈	4.80 ^{0.37} _{0.28}
52892	28	7440 ⁶¹² ₅₀₆	4.29 ^{0.37} _{0.27}
52894	30	7440 ⁵⁸¹ ₅₀₈	3.91 ^{0.29} _{0.22}
52896	32	7400 ⁵²² ₄₆₂	3.58 ^{0.25} _{0.20}

Table A1 – *continued* A List of the Temperatures and Bolometric Luminosities

52898	34	6980 ⁴⁴⁴ ₃₉₄	3.25 ^{0.18} _{0.14}
52900	36	6700 ⁴⁵⁹ ₄₀₀	3.00 ^{0.15} _{0.12}
52902	38	6505 ⁹⁶⁵ ₅₆₀	2.78 ^{0.41} _{0.17}
52904	40	6660 ⁹⁴⁵ ₇₂₉	2.70 ^{0.38} _{0.21}
52906	42	6740 ¹⁰⁰⁷ ₇₆₅	2.60 ^{0.39} _{0.22}
52910	46	6380 ⁸⁹⁶ ₆₇₁	2.40 ^{0.29} _{0.16}
52913	49	6220 ⁹³⁶ ₇₂₃	2.31 ^{0.28} _{0.16}
52919	55	6780 ¹²⁰⁵ ₈₆₅	2.07 ^{0.40} _{0.21}
SN2003hk			
52873	13	10500 ⁵⁸² ₅₁₃	4.17 ^{0.35} _{0.28}
52875	15	9600 ⁴⁷⁹ ₄₁₉	3.80 ^{0.25} _{0.21}
52877	17	9360 ⁴⁴⁵ ₄₀₃	3.57 ^{0.21} _{0.19}
52880	20	8660 ³⁷⁴ ₃₄₁	3.11 ^{0.15} _{0.13}
52881	21	8680 ³⁷⁵ ₃₄₃	2.99 ^{0.15} _{0.12}
52883	23	8720 ³⁷⁸ ₃₄₇	2.77 ^{0.14} _{0.12}
52885	25	8507 ⁶⁷⁰ ₆₂₆	2.53 ^{0.26} _{0.21}
52887	27	8580 ⁷²⁵ ₆₀₈	2.43 ^{0.27} _{0.20}
52889	29	8280 ¹¹⁹¹ ₈₇₈	2.29 ^{0.42} _{0.24}
52893	33	8560 ¹⁰²⁵ ₇₉₈	2.22 ^{0.39} _{0.26}
52900	40	7620 ⁶⁸¹ ₅₉₀	1.63 ^{0.18} _{0.13}
52903	43	7260 ⁴⁸² ₄₃₃	1.50 ^{0.10} _{0.07}
52906	46	7140 ⁴⁶⁷ ₄₁₅	1.42 ^{0.08} _{0.07}
52910	50	6760 ⁴²² ₃₆₂	1.30 ^{0.06} _{0.05}
52913	53	6480 ³⁷⁷ ₃₃₆	1.20 ^{0.05} _{0.04}
52916	56	6500 ³⁹⁰ ₃₃₀	1.16 ^{0.05} _{0.04}
52919	59	6480 ³⁷² ₃₄₀	1.14 ^{0.05} _{0.04}
52922	62	6460 ⁴⁷⁰ ₃₉₁	1.14 ^{0.06} _{0.05}
52928	68	5440 ³⁵⁸ ₃₁₁	1.07 ^{0.04} _{0.04}
52931	71	5960 ³²⁰ ₂₉₃	1.00 ^{0.03} _{0.03}
52935	75	5840 ²⁹⁹ ₂₈₆	0.93 ^{0.03} _{0.03}
52943	83	5300 ³³¹ ₂₉₄	0.79 ^{0.03} _{0.03}
52948	88	5760 ⁴²⁹ ₃₈₀	0.75 ^{0.03} _{0.03}
SN2003iq			
52922	2	12940 ⁹³² ₈₁₉	1.84 ^{0.25} _{0.20}
52927	7	9620 ⁴⁶⁰ ₄₃₈	1.83 ^{0.12} _{0.10}
52930	10	9260 ⁴³⁷ ₃₉₂	1.72 ^{0.10} _{0.09}
52933	13	8700 ³⁷⁶ ₃₄₅	1.54 ^{0.07} _{0.07}
52936	16	8111 ⁶⁰¹ ₅₆₃	1.45 ^{0.13} _{0.11}
52939	19	8080 ⁶¹⁹ ₅₄₃	1.49 ^{0.14} _{0.11}
52942	22	7880 ⁵⁹⁸ ₅₀₃	1.45 ^{0.12} _{0.09}
52945	25	7680 ⁵⁷² ₄₇₀	1.38 ^{0.11} _{0.08}
52948	28	7560 ⁵⁴¹ ₄₆₃	1.32 ^{0.10} _{0.07}
52955	35	6680 ⁴¹⁵ ₃₅₀	1.21 ^{0.06} _{0.04}

Table A1 – *continued* A List of the Temperatures and Bolometric Luminosities

52960	40	6280 ⁴³⁰ ₃₇₇	1.20 ^{0.04} _{0.04}
52963	43	6860 ⁴³⁷ ₃₇₂	1.19 ^{0.06} _{0.05}
52966	46	6520 ³⁷³ ₃₄₈	1.15 ^{0.05} _{0.04}
52969	49	6540 ³⁹⁸ ₃₃₂	1.13 ^{0.05} _{0.04}
52972	52	6240 ³⁵² ₃₀₅	1.13 ^{0.04} _{0.03}
52977	57	5560 ³²⁹ ₂₈₄	1.15 ^{0.04} _{0.03}
52992	72	6000 ³⁰⁹ ₂₉₂	0.99 ^{0.03} _{0.03}
52996	76	5980 ³²⁴ ₂₇₆	0.94 ^{0.03} _{0.03}
53002	82	5980 ³⁰⁷ ₂₉₀	0.88 ^{0.03} _{0.02}
53017	97	5580 ¹¹⁷⁰ ₈₀₂	0.56 ^{0.06} _{0.04}
53023	103	5020 ²³² ₂₁₆	0.38 ^{0.02} _{0.01}
53026	106	5040 ²²⁴ ₁₉₃	0.29 ^{0.01} _{0.01}
53042	122	5120 ⁵⁵⁵ ₄₆₁	0.20 ^{0.01} _{0.01}
53045	125	4620 ²⁵⁶ ₂₂₃	0.20 ^{0.01} _{0.01}
53048	128	4520 ²⁰⁶ ₂₀₃	0.20 ^{0.01} _{0.01}

SN2003z

52670	5	12020 ⁷⁸³ ₆₉₈	0.22 ^{0.03} _{0.02}
52671	6	12300 ⁸³¹ ₇₂₉	0.24 ^{0.03} _{0.02}
52674	9	10320 ⁵⁵⁶ ₄₉₇	0.19 ^{0.01} _{0.01}
52676	11	9520 ⁴⁶⁷ ₄₁₄	0.17 ^{0.01} _{0.01}
52679	14	8740 ¹⁸⁰² ₄₇₇	0.15 ^{0.05} _{0.01}
52691	26	7200 ⁷⁵⁵ ₆₀₆	0.12 ^{0.01} _{0.01}
52694	29	7380 ⁵⁰⁶ ₄₄₃	0.12 ^{0.01} _{0.01}
52701	36	7180 ⁴⁷³ ₄₁₉	0.13 ^{0.01} _{0.01}
52704	39	7040 ⁴⁴⁸ ₄₀₅	0.12 ^{0.01} _{0.01}
52707	42	6700 ⁴¹² ₃₅₅	0.12 ^{0.01} _{0.00}
52712	47	7560 ⁶⁸¹ ₅₇₄	0.15 ^{0.02} _{0.01}
52717	52	6860 ¹³⁷⁸ ₉₅₄	0.14 ^{0.03} _{0.02}
52722	57	6280 ⁷⁸¹ ₆₀₆	0.12 ^{0.01} _{0.01}
52727	62	5900 ³⁰⁶ ₂₇₅	0.12 ^{0.00} _{0.00}
52734	69	6220 ³⁵¹ ₃₂₄	0.12 ^{0.00} _{0.00}
52739	74	5600 ²⁶² ₂₅₆	0.11 ^{0.00} _{0.00}
52751	86	6180 ⁴³⁸⁴ ₁₇₀₇	0.11 ^{0.04} _{0.01}
52766	101	4840 ⁸²⁴ ₆₀₅	0.10 ^{0.01} _{0.01}
52771	106	5640 ³²³ ₂₉₀	0.09 ^{0.00} _{0.00}
52778	113	5900 ³¹⁵ ₂₈₉	0.07 ^{0.00} _{0.00}

SN2004A

53018	11	7960 ³⁶⁹ ₃₃₇	1.06 ^{0.04} _{0.04}
53032	25	6360 ¹⁹⁷ ₁₉₂	0.90 ^{0.02} _{0.02}
53037	30	6022 ⁵⁹² ₅₁₀	0.87 ^{0.03} _{0.03}
53045	38	5860 ⁵²⁹ ₄₃₈	0.88 ^{0.04} _{0.03}
53050	43	5860 ⁴⁰⁹ ₃₄₈	0.89 ^{0.03} _{0.03}
53052	45	5900 ³²⁹ ₂₉₇	0.89 ^{0.03} _{0.02}

Table A1 – *continued* A List of the Temperatures and Bolometric Luminosities

53065	58	5740 ³⁰⁹ ₂₈₂	0.90 ^{0.02} _{0.02}
53066	59	5760 ³²⁰ ₂₇₆	0.91 ^{0.02} _{0.02}
53076	69	5700 ³⁰⁰ ₂₈₁	0.91 ^{0.02} _{0.02}
53081	74	5710 ³⁰⁹ ₂₇₇	0.90 ^{0.03} _{0.03}
53099	92	5620 ³⁰² ₂₆₄	0.82 ^{0.02} _{0.02}
SN2004du			
53231	3	14644 ²⁹⁰³ ₁₆₅₈	4.53 ^{1.64} _{0.75}
53233	5	11420 ⁷⁰⁰ ₆₂₀	3.61 ^{0.36} _{0.30}
53235	7	10140 ⁵³⁹ ₄₇₅	3.35 ^{0.25} _{0.21}
53237	9	9500 ⁴⁵⁸ ₄₁₈	3.21 ^{0.20} _{0.17}
53239	11	9120 ⁴¹⁹ ₃₈₁	3.06 ^{0.17} _{0.15}
53242	14	8900 ³⁹⁷ ₃₆₁	2.93 ^{0.15} _{0.13}
53244	16	8680 ³⁷⁰ ₃₄₇	2.70 ^{0.13} _{0.11}
53246	18	8500 ⁴⁵⁷ ₄₁₅	2.55 ^{0.14} _{0.12}
53250	22	8153 ⁷⁰⁷ ₄₉₉	2.31 ^{0.25} _{0.15}
53251	23	8160 ⁶⁵⁰ ₅₄₂	2.26 ^{0.22} _{0.16}
53253	25	8120 ⁶²⁵ ₅₄₉	2.21 ^{0.20} _{0.16}
53255	27	8040 ⁶¹¹ ₅₃₇	2.18 ^{0.20} _{0.15}
53257	29	7920 ⁶¹⁰ ₅₀₅	2.13 ^{0.19} _{0.14}
53259	31	7780 ⁵⁹⁰ ₄₈₃	2.07 ^{0.17} _{0.13}
53263	35	7480 ⁵¹⁷ ₄₆₀	1.94 ^{0.14} _{0.11}
53265	37	7320 ⁴⁹⁵ ₄₃₇	1.88 ^{0.12} _{0.10}
53267	39	7180 ⁴⁸⁹ ₄₀₇	1.82 ^{0.12} _{0.08}
53269	41	7120 ⁴⁶⁵ ₄₁₁	1.79 ^{0.11} _{0.08}
53271	43	7060 ⁴⁶² ₄₀₀	1.75 ^{0.10} _{0.08}
53273	45	7160 ⁶⁷⁸ ₅₅₃	1.78 ^{0.17} _{0.11}
53276	48	6760 ⁴⁴⁹ ₄₀₆	1.65 ^{0.09} _{0.07}
53279	51	6420 ³⁷³ ₃₂₆	1.58 ^{0.06} _{0.05}
53282	54	6380 ³⁶⁶ ₃₂₃	1.57 ^{0.06} _{0.05}
53285	57	6360 ³⁶⁶ ₃₁₉	1.55 ^{0.06} _{0.05}
53288	60	6320 ³⁴⁴ ₃₂₈	1.53 ^{0.05} _{0.05}
53292	64	6180 ³³⁸ ₃₀₄	1.51 ^{0.05} _{0.04}
53301	73	5780 ³⁶² ₃₂₅	1.47 ^{0.05} _{0.04}
53309	81	5980 ³²¹ ₂₇₉	1.41 ^{0.04} _{0.04}
53329	101	5340 ³¹⁶ ₂₉₀	1.26 ^{0.04} _{0.04}
SN2004et			
53278	7	11580 ⁷⁷² ₆₇₇	2.42 ^{0.27} _{0.22}
53279	8	11280 ⁷¹⁵ ₆₄₈	2.39 ^{0.25} _{0.21}
53280	9	10900 ⁶⁶⁴ ₆₀₀	2.30 ^{0.22} _{0.18}
53281	10	10620 ⁶⁴⁸ ₅₄₈	2.22 ^{0.21} _{0.16}
53282	11	10380 ⁶¹⁰ ₅₂₅	2.15 ^{0.19} _{0.15}
53283	12	10140 ⁵⁶² ₅₁₂	2.09 ^{0.17} _{0.14}
53284	13	10020 ⁵⁴⁵ ₅₀₀	2.06 ^{0.16} _{0.14}

Table A1 – *continued* A List of the Temperatures and Bolometric Luminosities

53286	15	9750 ⁵³⁸ ₄₇₃	2.00 ^{0.15} _{0.12}
53287	16	9680 ⁵⁰⁷ ₄₆₂	1.98 ^{0.14} _{0.12}
53288	17	9600 ⁵⁰⁶ ₄₄₇	1.97 ^{0.14} _{0.11}
53289	18	9500 ⁵⁰⁰ ₄₃₂	1.96 ^{0.14} _{0.11}
53294	23	8300 ²⁰¹ ₁₉₅	1.65 ^{0.06} _{0.06}
53296	25	8021 ⁴¹¹ ₂₃₅	1.57 ^{0.14} _{0.07}
53297	26	7989 ³⁰⁶ ₂₆₄	1.58 ^{0.10} _{0.08}
53298	27	7880 ²⁴⁸ ₂₃₅	1.55 ^{0.08} _{0.07}
53299	28	7760 ²³⁹ ₂₀₉	1.51 ^{0.08} _{0.07}
53301	30	7600 ²¹⁴ ₂₁₃	1.46 ^{0.07} _{0.06}
53302	31	7340 ²¹² ₁₈₅	1.42 ^{0.07} _{0.06}
53306	35	7120 ¹⁶⁹ ₁₆₂	1.35 ^{0.05} _{0.05}
53307	36	7040 ¹⁷⁰ ₁₅₃	1.32 ^{0.05} _{0.05}
53309	38	6960 ¹⁷² ₁₄₅	1.30 ^{0.05} _{0.04}
53312	41	6860 ¹⁶⁰ ₁₄₆	1.27 ^{0.05} _{0.04}
53315	44	6740 ¹⁴¹ ₁₅₂	1.23 ^{0.04} _{0.04}
53316	45	6700 ¹⁴⁰ ₁₄₉	1.22 ^{0.04} _{0.04}
53317	46	6660 ¹⁴¹ ₁₄₄	1.20 ^{0.04} _{0.04}
53318	47	6640 ¹⁴⁰ ₁₄₃	1.20 ^{0.04} _{0.04}
53319	48	6610 ¹⁵³ ₁₄₄	1.19 ^{0.04} _{0.04}
53320	49	6590 ¹⁴⁶ ₁₄₁	1.19 ^{0.04} _{0.04}
53324	53	6520 ²⁴⁴ ₁₅₃	1.18 ^{0.08} _{0.04}
53326	55	6520 ¹⁹⁷ ₁₈₀	1.19 ^{0.06} _{0.06}
53327	56	6500 ¹⁹⁶ ₁₇₈	1.18 ^{0.21} _{0.11}
53328	57	6480 ¹⁹⁴ ₁₇₉	1.18 ^{0.06} _{0.06}
53329	58	6480 ¹⁹⁷ ₁₇₇	1.18 ^{0.06} _{0.06}
53330	59	6480 ¹⁸⁷ ₁₈₆	1.18 ^{0.06} _{0.06}
53331	60	6450 ¹⁹² ₁₈₇	1.17 ^{0.06} _{0.06}
53332	61	6420 ¹⁹¹ ₁₇₇	1.16 ^{0.06} _{0.06}
53333	62	6400 ¹⁹² ₁₇₃	1.16 ^{0.06} _{0.06}
53335	64	6360 ¹⁸⁶ ₁₈₁	1.14 ^{0.06} _{0.05}
53350	79	6480 ²⁵⁶ ₂₄₂	1.13 ^{0.33} _{0.15}
53353	82	6266 ³⁹⁵ ₂₆₀	1.08 ^{0.08} _{0.07}
53354	83	6340 ²¹⁹ ₂₁₁	1.08 ^{0.06} _{0.05}
53355	84	6320 ²³⁴ ₁₉₆	1.08 ^{0.06} _{0.05}
53375	104	6020 ¹⁶² ₁₅₃	0.84 ^{0.06} _{0.05}
53376	105	6080 ¹⁶⁰ ₁₆₁	0.83 ^{0.08} _{0.05}
53378	107	6020 ¹⁶² ₁₅₃	0.78 ^{0.06} _{0.04}
53381	110	5920 ¹⁴⁷ ₁₅₆	0.71 ^{0.26} _{0.14}
53406	135	5880 ²⁰⁵ ₁₉₄	0.20 ^{0.07} _{0.04}
53412	141	5940 ²¹⁴ ₂₀₃	0.17 ^{0.04} _{0.04}
SN2005cs			
53552	3	16327 ⁷⁴⁵ ₆₈₄	0.89 ^{0.08} _{0.07}
53553	4	15060 ⁸⁰¹ ₇₄₉	0.78 ^{0.08} _{0.07}

Table A1 – *continued* A List of the Temperatures and Bolometric Luminosities

53554	5	13509 ⁶⁹³ ₆₂₃	0.63 ^{0.06} _{0.05}
53555	6	12356 ⁸⁴⁶ ₆₉₂	0.54 ^{0.06} _{0.04}
53557	8	10418 ⁷⁸⁸ ₆₆₈	0.42 ^{0.03} _{0.03}
53558	9	9690 ³¹⁷ ₂₉₈	0.38 ^{0.02} _{0.02}
53559	10	9540 ²⁹⁵ ₂₇₁	0.38 ^{0.02} _{0.02}
53560	11	9269 ³⁷⁴ ₃₆₄	0.36 ^{0.02} _{0.02}
53562	13	8376 ⁴⁶⁸ ₃₃₃	0.31 ^{0.03} _{0.02}
53563	14	8088 ²⁴⁶ ₂₃₀	0.30 ^{0.02} _{0.02}
53564	15	7967 ²⁴⁷ ₂₂₀	0.29 ^{0.02} _{0.01}
53565	16	7708 ²⁴² ₂₁₉	0.27 ^{0.01} _{0.01}
53566	17	7560 ²⁴² ₂₁₇	0.27 ^{0.01} _{0.01}
53568	19	7360 ¹⁹⁵ ₁₉₁	0.26 ^{0.01} _{0.01}
53569	20	7260 ²⁰⁰ ₁₇₅	0.25 ^{0.01} _{0.01}
53571	22	6960 ¹⁹² ₁₇₇	0.24 ^{0.01} _{0.01}
53572	23	6920 ¹⁸⁶ ₁₇₈	0.24 ^{0.01} _{0.01}
53573	24	6967 ¹⁷⁵ ₁₇₆	0.24 ^{0.01} _{0.01}
53574	25	6880 ¹⁵⁹ ₁₄₇	0.24 ^{0.01} _{0.01}
53575	26	6700 ¹⁵⁰ ₁₄₂	0.24 ^{0.01} _{0.01}
53577	28	6720 ¹⁷⁸ ₁₅₀	0.24 ^{0.01} _{0.01}
53579	30	6670 ¹⁶⁷ ₁₆₂	0.24 ^{0.01} _{0.01}
53580	31	6760 ²⁰⁴ ₂₀₀	0.24 ^{0.01} _{0.01}
53583	34	6660 ¹⁸⁴ ₁₈₆	0.24 ^{0.01} _{0.01}
53584	35	6604 ²²⁷ ₁₈₀	0.25 ^{0.01} _{0.01}
53585	36	6505 ²⁰² ₁₈₀	0.24 ^{0.01} _{0.01}
53586	37	6700 ²⁵¹ ₂₂₈	0.26 ^{0.01} _{0.01}
53588	39	6560 ²³² ₂₂₅	0.26 ^{0.01} _{0.01}
53589	40	6500 ²²⁷ ₂₂₀	0.26 ^{0.01} _{0.01}
53591	42	6360 ¹⁹⁶ ₁₇₆	0.26 ^{0.01} _{0.01}
53593	44	6360 ¹⁸⁷ ₁₇₇	0.26 ^{0.02} _{0.01}
53595	46	6360 ²¹⁰ ₁₈₈	0.27 ^{0.02} _{0.02}
53599	50	6360 ¹⁸⁰ ₁₈₃	0.27 ^{0.01} _{0.01}
53600	51	6340 ¹⁸⁷ ₁₇₅	0.27 ^{0.01} _{0.01}
53605	56	6250 ¹⁹⁶ ₁₈₂	0.28 ^{0.02} _{0.01}
53606	57	6360 ¹⁸⁴ ₁₈₀	0.29 ^{0.01} _{0.01}
53610	61	6203 ²³⁰ ₂₄₇	0.28 ^{0.02} _{0.02}
53612	63	6260 ¹⁶⁸ ₁₇₅	0.29 ^{0.01} _{0.01}
53613	64	6320 ¹⁸⁴ ₁₈₁	0.30 ^{0.01} _{0.01}
53615	66	6310 ¹⁸² ₁₈₂	0.30 ^{0.01} _{0.01}
53617	68	6220 ¹⁶⁷ ₁₇₁	0.29 ^{0.01} _{0.01}
53619	70	6200 ¹⁸¹ ₁₅₆	0.29 ^{0.01} _{0.01}
53624	75	6100 ¹⁹⁹ ₁₉₆	0.29 ^{0.01} _{0.01}
53626	77	6240 ¹⁸⁵ ₁₅₇	0.30 ^{0.01} _{0.01}
53628	79	6220 ¹⁸² ₁₅₉	0.30 ^{0.01} _{0.01}
53629	80	6400 ⁹⁰⁶ ₆₈₇	0.33 ^{0.01} _{0.01}
53640	91	5520 ⁵⁶⁸ ₅₆₈	0.24 ^{0.01} _{0.01}

Table A1 – *continued* A List of the Temperatures and Bolometric Luminosities

53642	93	5520 ⁵⁸³ ₄₆₀	0.24 ^{0.02} _{0.01}
53781	232	4080 ³³⁸ ₂₈₃	0.01 ^{0.01} _{0.00}
SN2006bp			
53836	2	10662 ⁴⁸⁰ ₆₃₂	0.90 ^{0.06} _{0.06}
53837	3	9779 ²⁶⁷ ₂₀₈	0.91 ^{0.04} _{0.04}
53838	4	9380 ¹⁶³ ₁₅₂	0.95 ^{0.02} _{0.02}
53839	5	8713 ¹⁷¹ ₂₁₅	0.97 ^{0.02} _{0.02}
53840	6	8292 ²²⁵ ₁₇₃	0.97 ^{0.02} _{0.02}
53841	7	8085 ¹⁵⁸ ₁₅₅	0.96 ^{0.02} _{0.02}
53842	8	7796 ¹⁷⁵ ₁₆₉	0.95 ^{0.02} _{0.02}
53843	9	7447 ¹⁵⁰ ₁₃₅	0.93 ^{0.02} _{0.02}
53844	10	7176 ¹⁵⁶ ₂₆₉	0.92 ^{0.02} _{0.02}
53846	12	6724 ¹⁴³ ₁₃₀	0.89 ^{0.02} _{0.02}
53847	13	6640 ¹²⁴ ₁₂₆	0.88 ^{0.02} _{0.02}
53848	14	6513 ¹⁶⁹ ₁₇₀	0.87 ^{0.02} _{0.02}
53849	15	6360 ²³¹ ₂₁₅	0.85 ^{0.02} _{0.02}
53850	16	6290 ²⁰³ ₁₉₀	0.84 ^{0.02} _{0.02}
53852	18	6050 ¹⁸¹ ₁₈₆	0.84 ^{0.02} _{0.02}
53854	20	5782 ⁴⁶⁷ ₁₉₈	0.83 ^{0.02} _{0.02}
53857	23	5880 ³⁶⁵ ₃₁₃	0.84 ^{0.02} _{0.02}
53858	24	5840 ³⁴⁵ ₃₁₄	0.84 ^{0.02} _{0.02}
53859	25	5740 ³³⁸ ₂₉₈	0.84 ^{0.02} _{0.02}
53860	26	5680 ³³⁵ ₂₉₁	0.83 ^{0.02} _{0.02}
53861	27	5560 ³¹⁴ ₂₈₅	0.83 ^{0.03} _{0.02}
53862	28	5580 ³¹² ₂₉₂	0.83 ^{0.03} _{0.02}
53866	32	5420 ²⁹⁷ ₂₇₃	0.81 ^{0.03} _{0.02}
53867	33	5340 ²⁹⁴ ₂₅₃	0.81 ^{0.03} _{0.02}
53870	36	5300 ²⁷¹ ₂₆₄	0.78 ^{0.03} _{0.02}
53886	52	4960 ²⁴⁸ ₂₂₉	0.74 ^{0.04} _{0.03}
SN2007od			
54410	11	8720 ⁵⁸² ₅₀₄	6.60 ^{0.37} _{0.31}
54411	12	8640 ⁵⁷⁷ ₅₂₀	6.55 ^{0.36} _{0.32}
54412	13	8420 ³⁵⁵ ₃₃₀	6.55 ^{0.32} _{0.29}
54413	14	8500 ³³⁰ ₂₈₈	6.34 ^{0.30} _{0.24}
54414	15	8386 ¹⁹⁵ ₁₈₀	6.17 ^{0.37} _{0.25}
54416	17	8140 ¹⁵³ ₁₅₇	5.72 ^{0.22} _{0.21}
54417	18	8000 ¹⁸⁸ ₁₈₀	5.49 ^{0.24} _{0.24}
54418	19	7904 ²⁰³ ₂₃₃	5.34 ^{0.26} _{0.29}
54422	23	7846 ²⁹⁹ ₂₂₃	5.18 ^{0.45} _{0.28}
54426	27	7680 ²⁰¹ ₁₇₂	4.96 ^{0.23} _{0.19}
54428	29	7600 ¹⁸⁶ ₁₈₄	4.79 ^{0.21} _{0.20}
54429	30	7580 ¹⁸⁶ ₁₇₆	4.75 ^{0.21} _{0.19}
54433	34	7500 ¹⁸⁷ ₁₆₇	4.56 ^{0.19} _{0.18}

Table A1 – *continued* A List of the Temperatures and Bolometric Luminosities

54436	37	7420 ²⁰¹ ₁₉₂	4.46 ^{0.22} _{0.20}
54439	40	7150 ²⁴⁵ ₂₃₂	4.12 ^{0.27} _{0.23}
54441	42	7060 ¹⁶¹ ₁₆₈	3.99 ^{0.15} _{0.16}
54442	43	7000 ¹⁴⁵ ₁₅₄	3.91 ^{0.13} _{0.14}
54446	47	6860 ¹³⁷ ₁₄₈	3.70 ^{0.12} _{0.12}
54449	50	6690 ¹⁴⁹ ₁₄₆	3.46 ^{0.13} _{0.13}
54450	51	6800 ¹⁴⁶ ₁₅₂	3.54 ^{0.13} _{0.13}
54451	52	6800 ¹⁴⁹ ₁₅₅	3.54 ^{0.13} _{0.13}
54456	57	6660 ¹⁸⁴ ₁₆₇	3.40 ^{0.17} _{0.15}
54460	61	6446 ³¹⁹ ₁₉₀	3.05 ^{0.34} _{0.16}
54462	63	6440 ¹²⁸ ₁₃₈	2.96 ^{0.10} _{0.10}
54464	65	6600 ¹⁶⁰ ₁₄₄	3.06 ^{0.12} _{0.11}
54473	74	6720 ¹⁴⁹ ₁₃₁	2.48 ^{0.09} _{0.08}
<hr/>			
SN2008in			
<hr/>			
54830	8	10600 ¹⁹³ ₁₆₈	0.70 ^{0.02} _{0.02}
54831	9	9965 ⁷⁴¹ ₅₆₀	0.64 ^{0.07} _{0.05}
54833	11	9383 ⁵¹⁹ ₄₅₆	0.57 ^{0.04} _{0.03}
54835	13	9123 ⁴⁰¹ ₃₉₉	0.54 ^{0.03} _{0.03}
54839	17	7575 ³⁷¹ ₂₈₅	0.44 ^{0.03} _{0.02}
54841	19	7519 ³¹² ₂₈₂	0.45 ^{0.02} _{0.02}
54843	21	7540 ³⁴⁵ ₃₀₇	0.44 ^{0.02} _{0.02}
54846	24	7300 ³³⁸ ₃₀₃	0.42 ^{0.02} _{0.02}
54851	29	6919 ³⁵⁴ ₂₇₅	0.40 ^{0.02} _{0.01}
54855	33	6600 ²⁸⁴ ₂₅₆	0.38 ^{0.02} _{0.01}
54856	34	6420 ²¹² ₂₀₃	0.37 ^{0.01} _{0.01}
54858	36	6340 ¹⁹² ₁₈₃	0.36 ^{0.01} _{0.01}
54860	38	6320 ¹⁸³ ₁₈₅	0.36 ^{0.01} _{0.01}
54861	39	6240 ¹⁷⁵ ₁₄₉	0.36 ^{0.01} _{0.01}
54862	40	6240 ¹⁹⁸ ₁₇₀	0.36 ^{0.01} _{0.01}
54864	42	6220 ¹⁸⁵ ₁₇₆	0.36 ^{0.01} _{0.01}
54868	46	6140 ²⁰⁵ ₁₈₁	0.36 ^{0.01} _{0.01}
54874	52	6220 ²⁶⁶ ₂₆₁	0.35 ^{0.01} _{0.01}
54878	56	6100 ²⁴³ ₂₀₆	0.34 ^{0.01} _{0.01}
54879	57	6084 ³⁹⁶ ₂₄₁	0.34 ^{0.01} _{0.01}
54880	58	6240 ²²⁷ ₂₁₂	0.34 ^{0.01} _{0.01}
54883	61	6140 ²²⁹ ₁₉₇	0.33 ^{0.01} _{0.01}
54884	62	6180 ²¹³ ₁₉₅	0.33 ^{0.01} _{0.01}
54885	63	6170 ²²⁶ ₂₁₂	0.33 ^{0.01} _{0.01}
54886	64	6220 ²⁹⁹ ₂₆₇	0.33 ^{0.02} _{0.02}
54888	66	6180 ³⁰² ₂₅₈	0.32 ^{0.02} _{0.01}
54889	67	6060 ¹⁹⁷ ₁₈₂	0.31 ^{0.01} _{0.01}
54890	68	6060 ²⁰⁸ ₁₉₀	0.31 ^{0.01} _{0.01}
54893	71	6060 ²⁰⁹ ₂₀₆	0.30 ^{0.01} _{0.01}
54895	73	6021 ²³² ₂₃₈	0.30 ^{0.01} _{0.01}

Table A1 – *continued* A List of the Temperatures and Bolometric Luminosities

54900	78	5940 ²⁸⁶ ₂₇₁	0.29 ^{0.01} _{0.01}
54901	79	6460 ⁶⁷⁹ ₅₄₂	0.31 ^{0.03} _{0.02}
54906	84	5880 ²⁵⁷ ₂₄₆	0.28 ^{0.01} _{0.01}
54912	90	6000 ³³⁵ ₂₈₈	0.26 ^{0.01} _{0.01}
54915	93	5840 ¹⁹³ ₁₈₇	0.24 ^{0.01} _{0.01}
54917	95	5860 ¹⁹³ ₁₆₇	0.23 ^{0.01} _{0.01}
54925	103	5960 ²⁴⁸ ₂₂₅	0.20 ^{0.01} _{0.01}
54927	105	5649 ²⁵⁰ ₂₁₃	0.17 ^{0.01} _{0.00}
54932	110	5240 ²⁰⁷ ₂₀₄	0.12 ^{0.00} _{0.00}
54937	115	4279 ¹⁷⁰ ₂₈₁	0.08 ^{0.00} _{0.00}
SN2009N			
54858	13	10120 ⁸³⁵ ₇₁₁	0.57 ^{0.04} _{0.03}
54859	14	8154 ²⁵⁶ ₂₅₉	0.53 ^{0.02} _{0.02}
54860	15	8050 ²³⁶ ₂₂₀	0.53 ^{0.01} _{0.01}
54861	16	7895 ²³² ₂₁₇	0.52 ^{0.01} _{0.01}
54863	18	7220 ¹⁵⁴ ₁₄₃	0.50 ^{0.01} _{0.01}
54864	19	6940 ¹⁴⁸ ₁₄₂	0.49 ^{0.01} _{0.01}
54865	20	6600 ¹³⁸ ₁₂₃	0.49 ^{0.01} _{0.01}
54867	22	6413 ¹²⁰ ₉₇	0.47 ^{0.02} _{0.02}
54869	24	6320 ¹³⁵ ₁₃₄	0.47 ^{0.01} _{0.01}
54871	26	6160 ¹³² ₁₂₁	0.46 ^{0.01} _{0.01}
54872	27	6100 ¹¹⁸ ₁₃₀	0.46 ^{0.01} _{0.01}
54875	30	5900 ¹²³ ₁₁₃	0.46 ^{0.01} _{0.01}
54878	33	5800 ¹⁴⁸ ₁₂₄	0.47 ^{0.02} _{0.02}
54880	35	5750 ¹⁴⁰ ₁₃₀	0.48 ^{0.02} _{0.02}
54887	42	5500 ¹²² ₁₁₈	0.49 ^{0.02} _{0.01}
54888	43	5480 ¹²⁶ ₁₁₃	0.50 ^{0.02} _{0.01}
54889	44	5480 ¹²⁵ ₁₁₆	0.50 ^{0.01} _{0.01}
54890	45	5480 ¹¹⁴ ₁₂₄	0.50 ^{0.01} _{0.01}
54891	46	5460 ¹²⁰ ₁₁₇	0.51 ^{0.01} _{0.01}
54896	51	5340 ¹²³ ₁₀₄	0.52 ^{0.01} _{0.01}
54897	52	5340 ¹²³ ₁₀₃	0.52 ^{0.01} _{0.01}
54902	57	5320 ¹¹⁵ ₁₀₉	0.53 ^{0.01} _{0.01}
54904	59	5320 ¹²³ ₁₀₁	0.53 ^{0.01} _{0.01}
54906	61	5340 ¹¹⁴ ₁₁₂	0.54 ^{0.01} _{0.01}
54907	62	5360 ¹¹³ ₁₁₅	0.53 ^{0.01} _{0.01}
54908	63	5360 ¹¹³ ₁₁₄	0.53 ^{0.01} _{0.01}
54909	64	5360 ¹¹² ₁₁₆	0.53 ^{0.01} _{0.01}
54910	65	5340 ¹⁰⁹ ₁₁₆	0.54 ^{0.01} _{0.01}
54911	66	5320 ¹²⁴ ₁₀₁	0.54 ^{0.01} _{0.01}
54913	68	5320 ¹¹² ₁₁₄	0.54 ^{0.01} _{0.01}
54915	70	5300 ¹¹⁹ ₁₀₄	0.53 ^{0.01} _{0.01}
54916	71	5300 ¹¹² ₁₁₀	0.53 ^{0.01} _{0.01}
54917	72	5280 ¹²³ ₁₀₀	0.53 ^{0.01} _{0.01}

Table A1 – *continued* A List of the Temperatures and Bolometric Luminosities

54918	73	5280 ¹²⁰ ₁₀₁	0.53 ^{0.01} _{0.01}
54919	74	5280 ¹¹⁷ ₁₀₅	0.53 ^{0.01} _{0.01}
54920	75	5280 ¹¹⁵ ₁₀₅	0.53 ^{0.01} _{0.01}
54946	101	5300 ¹¹³ ₁₀₉	0.39 ^{0.01} _{0.01}
54947	102	5060 ¹⁰⁹ ₁₂₂	0.39 ^{0.01} _{0.01}
SN2009bw			
54923	6	15826 ⁹⁸⁸ ₇₅₇	2.29 ^{0.64} _{0.09}
54924	7	14043 ³⁶⁵ ₃₅₆	2.16 ^{0.08} _{0.08}
54925	8	11720 ²³³ ₂₃₈	1.73 ^{0.06} _{0.05}
54926	9	11022 ²⁹³ ₅₃₄	1.61 ^{0.08} _{0.10}
54927	10	10360 ³⁵⁰ ₃₃₇	1.47 ^{0.06} _{0.06}
54930	13	9240 ²⁹⁶ ₂₇₇	1.25 ^{0.05} _{0.04}
54931	14	9040 ²⁸¹ ₂₈₀	1.20 ^{0.04} _{0.04}
54932	15	8891 ³²⁴ ₃₂₈	1.16 ^{0.05} _{0.05}
54935	18	8324 ³³³ ₆₀₂	1.00 ^{0.04} _{0.07}
54937	20	7638 ²¹⁴ ₁₇₇	0.86 ^{0.02} _{0.02}
54942	25	7090 ⁵⁰² ₄₄₃	0.79 ^{0.05} _{0.04}
54945	28	6820 ⁴⁶² ₄₀₀	0.75 ^{0.04} _{0.03}
54946	29	6780 ⁴⁶⁵ ₃₈₆	0.74 ^{0.04} _{0.03}
54949	32	6500 ⁴⁰⁴ ₃₆₇	0.68 ^{0.03} _{0.03}
54951	34	6840 ¹⁷⁴⁴ ₁₁₃₀	0.67 ^{0.19} _{0.08}
54952	35	6560 ⁴³⁰ ₃₆₂	0.64 ^{0.03} _{0.02}
54953	36	6400 ³⁹⁵ ₃₅₂	0.62 ^{0.03} _{0.02}
54956	39	5950 ³⁴⁰ ₃₁₀	0.59 ^{0.02} _{0.02}
54957	40	5760 ⁴⁹⁷ ₄₂₅	0.59 ^{0.02} _{0.02}
54961	44	5680 ⁴²⁴ ₃₅₄	0.56 ^{0.02} _{0.02}
54967	50	5480 ³⁸³ ₃₂₄	0.55 ^{0.02} _{0.02}
54971	54	5420 ²⁸⁸ ₂₄₆	0.52 ^{0.02} _{0.02}
54974	57	5420 ²⁷⁹ ₂₄₄	0.52 ^{0.01} _{0.01}
54978	61	5400 ⁶⁶¹ ₅₁₆	0.51 ^{0.03} _{0.04}
54979	62	5460 ⁹³⁵ ₆₉₂	0.52 ^{0.04} _{0.03}
54983	66	5600 ²⁸⁹ ₂₇₀	0.51 ^{0.01} _{0.01}
54984	67	5540 ²⁹²⁹ ₁₄₀₆	0.51 ^{0.23} _{0.05}
55010	93	5450 ¹⁰⁷⁹ ₂₉₅	0.45 ^{0.05} _{0.01}
55033	116	5720 ⁷³¹ ₅₈₁	0.36 ^{0.03} _{0.02}
55037	120	5800 ⁷⁶⁵ ₅₉₀	0.34 ^{0.03} _{0.02}
55040	123	5900 ¹⁰⁸⁰ ₇₉₂	0.33 ^{0.04} _{0.02}
55044	127	6236 ¹⁹²⁰ ₁₂₉₇	0.31 ^{0.10} _{0.03}
55050	133	8500 ⁴⁹²⁵ ₂₁₈₃	0.26 ^{0.32} _{0.07}
SN2009ib			
55054	13	9120 ¹⁸⁸ ₂₀₀	0.76 ^{0.02} _{0.02}
55056	15	8192 ¹⁰³¹ ₃₅₁	0.67 ^{0.09} _{0.02}
55057	16	8104 ¹⁰⁴¹ ₃₉₄	0.66 ^{0.14} _{0.04}

Table A1 – *continued* A List of the Temperatures and Bolometric Luminosities

55063	22	7860 ⁶²⁶ ₅₁₉	0.65 ^{0.10} _{0.07}
55064	23	7760 ⁵⁹⁰ ₄₉₆	0.64 ^{0.07} _{0.05}
55066	25	7330 ⁵⁴³ ₄₄₄	0.60 ^{0.07} _{0.04}
55067	26	7340 ⁵¹² ₄₅₃	0.60 ^{0.05} _{0.04}
55068	27	7109 ⁵⁰⁹ ₄₀₉	0.57 ^{0.05} _{0.04}
55069	28	7150 ⁴⁷⁹ ₄₁₀	0.59 ^{0.04} _{0.04}
55070	29	6920 ⁴²⁰ ₃₇₉	0.55 ^{0.04} _{0.03}
55071	30	6840 ⁴¹⁵ ₃₆₅	0.55 ^{0.04} _{0.03}
55072	31	6818 ⁴⁸¹ ₄₁₄	0.55 ^{0.04} _{0.04}
55073	32	6640 ³⁵⁷ ₃₀₈	0.54 ^{0.04} _{0.03}
55074	33	6660 ³⁷⁷ ₃₃₅	0.53 ^{0.03} _{0.02}
55075	34	6640 ³⁸¹ ₃₃₀	0.54 ^{0.03} _{0.03}
55077	36	6380 ³⁴⁶ ₃₀₃	0.51 ^{0.03} _{0.02}
55079	38	6340 ³³² ₃₁₀	0.51 ^{0.03} _{0.02}
55082	41	6260 ³¹⁹ ₃₀₃	0.51 ^{0.02} _{0.02}
55083	42	6120 ³¹² ₂₈₄	0.50 ^{0.02} _{0.02}
55084	43	6139 ³⁴¹ ₃₀₁	0.50 ^{0.02} _{0.02}
55085	44	6130 ³²² ₂₇₈	0.50 ^{0.03} _{0.02}
55086	45	6140 ³⁰⁴ ₂₉₀	0.50 ^{0.02} _{0.02}
55087	46	6140 ³²¹ ₂₈₄	0.51 ^{0.02} _{0.02}
55088	47	6100 ³⁰² ₂₇₃	0.50 ^{0.02} _{0.02}
55089	48	5940 ²³⁹ ₂₂₁	0.49 ^{0.02} _{0.02}
55090	49	5950 ²⁹⁰ ₂₇₄	0.49 ^{0.02} _{0.02}
55091	50	5900 ²⁹⁰ ₂₆₅	0.49 ^{0.02} _{0.02}
55092	51	5870 ³⁰¹ ₂₇₀	0.49 ^{0.02} _{0.02}
55093	52	5880 ²⁸⁹ ₂₆₂	0.49 ^{0.02} _{0.02}
55094	53	5880 ²⁸² ₂₅₁	0.49 ^{0.02} _{0.02}
55095	54	5745 ⁵¹⁴ ₃₁₈	0.48 ^{0.02} _{0.02}
55096	55	5960 ³¹⁸ ₂₇₃	0.49 ^{0.02} _{0.01}
55097	56	5940 ³⁰⁷ ₂₇₈	0.49 ^{0.02} _{0.01}
55099	58	5840 ³⁰⁰ ₂₆₅	0.48 ^{0.02} _{0.02}
55100	59	5870 ³²² ₂₉₄	0.48 ^{0.02} _{0.01}
55104	63	5840 ³⁰⁵ ₂₈₆	0.49 ^{0.02} _{0.01}
55105	64	5820 ³¹⁶ ₂₇₂	0.49 ^{0.02} _{0.01}
55109	68	5760 ³⁰⁴ ₂₇₁	0.48 ^{0.02} _{0.01}
55111	70	5720 ³⁰⁸ ₂₅₉	0.48 ^{0.02} _{0.01}
55116	75	5360 ²⁰³ ₁₉₁	0.47 ^{0.02} _{0.01}
55117	76	5520 ²⁵¹ ₂₃₇	0.48 ^{0.02} _{0.01}
55121	80	5540 ²⁵⁰ ₂₃₄	0.48 ^{0.02} _{0.01}
55122	81	5520 ²³⁴ ₂₃₀	0.48 ^{0.01} _{0.01}
55124	83	5500 ²⁴⁴ ₂₁₈	0.48 ^{0.01} _{0.01}
55128	87	5260 ¹⁴⁶ ₁₅₄	0.48 ^{0.01} _{0.01}
55131	90	5500 ²³² ₂₂₇	0.48 ^{0.01} _{0.01}
55132	91	5480 ²⁴⁴ ₂₁₄	0.48 ^{0.01} _{0.01}
55134	93	5480 ²⁴¹ ₂₁₆	0.48 ^{0.01} _{0.01}

Table A1 – *continued* A List of the Temperatures and Bolometric Luminosities

55137	96	5480 ²³⁷ ₂₁₉	0.48 ^{0.01} _{0.01}
55138	97	5460 ²³⁹ ₂₁₄	0.48 ^{0.01} _{0.01}
55141	100	5520 ²⁵⁹ ₂₃₀	0.48 ^{0.01} _{0.01}
55146	105	5460 ²⁴² ₂₀₉	0.47 ^{0.01} _{0.01}
55147	106	5460 ²³⁷ ₂₁₃	0.47 ^{0.01} _{0.01}
SN2012A			
55937	8	15960 ⁶³⁶ ₅₉₄	1.62 ^{0.12} _{0.11}
55938	9	13700 ¹¹⁶⁶ ₆₄₁	1.43 ^{0.21} _{0.14}
55939	10	12039 ⁵⁶⁷ ₅₀₃	1.17 ^{0.08} _{0.07}
55940	11	11043 ⁴⁶⁴ ₉₆₁	1.06 ^{0.09} _{0.15}
55941	12	10837 ⁷¹⁰ ₆₀₀	1.04 ^{0.16} _{0.11}
55942	13	10665 ⁴⁸² ₄₃₂	1.04 ^{0.08} _{0.06}
55943	14	10459 ⁵³⁵ ₄₄₁	1.02 ^{0.08} _{0.06}
55945	16	10106 ⁴⁷³ ₄₂₈	0.98 ^{0.07} _{0.06}
55948	19	9034 ⁷⁰⁹ ₆₅₃	0.82 ^{0.10} _{0.07}
55949	20	9020 ⁶⁷¹ ₅₇₂	0.82 ^{0.09} _{0.07}
55951	22	8680 ⁷⁸⁷ ₆₆₁	0.79 ^{0.10} _{0.07}
55952	23	8577 ⁸⁰³ ₆₃₃	0.78 ^{0.11} _{0.07}
55953	24	8261 ¹¹⁰⁵ ₆₂₂	0.73 ^{0.17} _{0.07}
55954	25	7960 ⁴⁹⁰ ₄₁₆	0.70 ^{0.05} _{0.04}
55955	26	7800 ⁴⁹² ₄₁₆	0.68 ^{0.05} _{0.04}
55957	28	7620 ⁴⁰³ ₃₈₄	0.64 ^{0.04} _{0.03}
55958	29	7519 ⁴⁸⁴ ₃₉₈	0.63 ^{0.05} _{0.03}
55962	33	7540 ⁴⁵³ ₄₀₈	0.63 ^{0.05} _{0.04}
55966	37	7099 ⁶⁷⁰ ₄₅₀	0.58 ^{0.07} _{0.04}
55967	38	7194 ⁵⁵² ₅₁₉	0.59 ^{0.05} _{0.05}
55969	40	7179 ⁶⁰⁶ ₃₆₅	0.58 ^{0.05} _{0.03}
55972	43	7320 ⁵³⁸ ₄₅₃	0.58 ^{0.05} _{0.04}
55974	45	7320 ⁵⁷¹ ₄₇₂	0.58 ^{0.05} _{0.04}
55975	46	7235 ⁵⁹² ₄₄₂	0.58 ^{0.05} _{0.04}
55976	47	7220 ⁵⁰⁹ ₄₃₆	0.57 ^{0.05} _{0.04}
55977	48	7160 ⁵⁰⁴ ₄₂₂	0.57 ^{0.04} _{0.03}
55979	50	6959 ⁴⁸⁸ ₄₀₄	0.54 ^{0.04} _{0.03}
55981	52	6940 ⁵⁰³ ₄₀₈	0.53 ^{0.04} _{0.03}
55982	53	6940 ⁵⁰⁹ ₄₃₇	0.52 ^{0.04} _{0.03}
55983	54	6840 ⁴⁸³ ₄₀₄	0.52 ^{0.04} _{0.03}
55984	55	6840 ⁴⁶⁸ ₄₁₉	0.52 ^{0.04} _{0.03}
55985	56	6940 ⁴⁹¹ ₄₁₃	0.52 ^{0.04} _{0.03}
55987	58	6680 ⁴⁶⁷ ₄₀₄	0.49 ^{0.04} _{0.03}
55988	59	6420 ⁴¹⁴ ₃₆₃	0.47 ^{0.03} _{0.02}
55991	62	6520 ⁴⁴¹ ₃₉₁	0.48 ^{0.03} _{0.03}
55992	63	6680 ⁴⁰¹ ₃₅₄	0.49 ^{0.03} _{0.02}
55993	64	6760 ³⁹¹ ₃₅₅	0.50 ^{0.03} _{0.03}
55994	65	6820 ³⁹² ₃₆₅	0.50 ^{0.03} _{0.03}

Table A1 – *continued* A List of the Temperatures and Bolometric Luminosities

55999	70	6653 ⁴¹⁹ ₃₅₀	0.46 ^{0.03} _{0.03}
56000	71	6580 ³⁶¹ ₃₂₀	0.46 ^{0.02} _{0.02}
56001	72	6665 ³⁶¹ ₃₂₈	0.45 ^{0.03} _{0.02}
56002	73	6657 ⁴³¹ ₃₄₀	0.43 ^{0.03} _{0.02}
56003	74	6600 ³²⁸ ₂₈₉	0.43 ^{0.02} _{0.02}
56004	75	6600 ³²⁹ ₃₀₆	0.43 ^{0.02} _{0.02}
56005	76	6620 ³²³ ₂₉₁	0.42 ^{0.02} _{0.02}
56006	77	6600 ²⁸⁰ ₂₆₆	0.42 ^{0.02} _{0.02}
56008	79	6600 ²⁹⁴ ₂₇₀	0.41 ^{0.02} _{0.02}
56009	80	6590 ³⁰⁶ ₂₇₉	0.40 ^{0.02} _{0.02}
56010	81	6680 ³²² ₂₈₃	0.40 ^{0.02} _{0.02}
56011	82	6700 ³⁴⁵ ₃₀₃	0.39 ^{0.02} _{0.02}
56012	83	6560 ²³⁶ ₂₀₄	0.38 ^{0.02} _{0.01}
56014	85	6600 ²⁴⁹ ₂₂₀	0.37 ^{0.04} _{0.03}
56015	86	6640 ²³⁵ ₂₃₄	0.36 ^{0.02} _{0.01}
56016	87	6600 ²³² ₂₁₅	0.35 ^{0.02} _{0.02}
56017	88	6587 ²⁴² ₂₂₀	0.34 ^{0.02} _{0.02}
56019	90	6600 ²³⁶ ₂₀₃	0.33 ^{0.02} _{0.01}
56021	92	6600 ²³⁴ ₂₁₈	0.32 ^{0.01} _{0.01}
56023	94	6700 ²¹¹ ₁₉₅	0.30 ^{0.01} _{0.01}
56027	98	6725 ³³⁹ ₂₈₃	0.28 ^{0.02} _{0.02}
56030	101	6600 ²⁷¹ ₂₆₅	0.24 ^{0.01} _{0.02}
56031	102	6400 ²³⁸ ₂₂₅	0.22 ^{0.01} _{0.01}
56033	104	6280 ²⁵² ₂₃₇	0.20 ^{0.01} _{0.01}
56034	105	6240 ¹⁹⁷ ₁₈₄	0.19 ^{0.01} _{0.01}
56035	106	6200 ²³² ₂₁₄	0.18 ^{0.01} _{0.01}
56037	108	6100 ²¹⁶ ₂₀₉	0.16 ^{0.01} _{0.01}
56039	110	5540 ²¹² ₁₈₆	0.12 ^{0.01} _{0.01}
SN2012aw			
56006	4	14235 ¹¹⁵³ ₆₇₅	2.60 ^{0.28} _{0.17}
56007	5	13752 ⁵⁵⁶ ₅₀₈	2.53 ^{0.15} _{0.13}
56008	6	12549 ⁶⁰⁷ ₅₂₇	2.34 ^{0.14} _{0.11}
56009	7	11889 ⁴⁹¹ ₄₈₁	2.25 ^{0.12} _{0.09}
56010	8	11479 ⁴²³ ₃₇₁	2.22 ^{0.09} _{0.08}
56011	9	11239 ⁵⁷¹ ₅₆₇	2.20 ^{0.17} _{0.14}
56012	10	10805 ³²⁹ ₃₀₉	2.09 ^{0.09} _{0.08}
56013	11	10639 ³²⁰ ₂₉₈	2.04 ^{0.08} _{0.07}
56014	12	10214 ³³³ ₂₉₆	1.97 ^{0.08} _{0.07}
56015	13	9760 ²¹⁹ ₂₀₅	1.85 ^{0.05} _{0.04}
56016	14	9553 ³²⁰ ₃₉₈	1.80 ^{0.07} _{0.09}
56017	15	9139 ²⁸⁸ ₂₆₂	1.70 ^{0.06} _{0.05}
56018	16	8930 ²⁵¹ ₂₀₃	1.67 ^{0.04} _{0.04}
56019	17	8454 ³⁷⁹ ₄₆₄	1.60 ^{0.05} _{0.07}
56020	18	7980 ¹³⁷ ₁₂₆	1.55 ^{0.05} _{0.04}

Table A1 – *continued* A List of the Temperatures and Bolometric Luminosities

56022	20	7640 ¹²⁴ ₁₁₁	1.49 ^{0.04} _{0.04}
56024	22	7400 ¹²⁷ ₁₂₄	1.46 ^{0.04} _{0.04}
56025	23	7377 ¹⁸² ₂₂₆	1.46 ^{0.06} _{0.06}
56026	24	7260 ¹⁵⁹ ₁₆₅	1.43 ^{0.06} _{0.05}
56027	25	7160 ¹⁶⁰ ₁₅₀	1.40 ^{0.06} _{0.05}
56028	26	7120 ¹⁴⁸ ₁₅₆	1.40 ^{0.06} _{0.05}
56029	27	7020 ¹⁶² ₁₄₄	1.37 ^{0.05} _{0.05}
56030	28	6965 ¹⁷⁷ ₁₈₀	1.36 ^{0.05} _{0.05}
56031	29	6880 ¹⁴⁶ ₁₄₈	1.34 ^{0.05} _{0.05}
56032	30	6792 ¹⁸⁴ ₁₄₇	1.33 ^{0.05} _{0.05}
56033	31	6740 ¹³⁶ ₁₄₁	1.32 ^{0.04} _{0.04}
56034	32	6700 ¹³⁴ ₁₃₆	1.31 ^{0.04} _{0.04}
56035	33	6628 ¹⁷⁶ ₁₄₃	1.30 ^{0.05} _{0.04}
56036	34	6621 ²¹⁰ ₂₂₉	1.28 ^{0.05} _{0.05}
56037	35	6540 ²⁰⁷ ₂₀₈	1.27 ^{0.05} _{0.04}
56039	37	6440 ²⁰⁴ ₁₉₇	1.26 ^{0.05} _{0.04}
56040	38	6425 ²¹² ₁₉₆	1.27 ^{0.05} _{0.05}
56041	39	6438 ²⁶⁴ ₂₂₅	1.27 ^{0.05} _{0.05}
56042	40	6440 ²¹⁸ ₁₈₉	1.28 ^{0.06} _{0.04}
56043	41	6380 ¹⁷⁸ ₁₇₆	1.28 ^{0.05} _{0.05}
56044	42	6360 ¹⁷⁹ ₁₇₃	1.28 ^{0.05} _{0.05}
56046	44	6280 ¹⁷⁷ ₁₆₆	1.27 ^{0.05} _{0.05}
56047	45	6233 ¹⁸³ ₁₇₂	1.26 ^{0.05} _{0.04}
56049	47	6160 ¹⁶⁸ ₁₅₉	1.25 ^{0.05} _{0.05}
56050	48	6100 ¹²⁸ ₁₃₈	1.26 ^{0.05} _{0.04}
56051	49	6000 ¹⁶⁰ ₁₅₃	1.25 ^{0.05} _{0.04}
56052	50	5813 ¹⁶⁵ ₁₄₇	1.24 ^{0.04} _{0.04}
56053	51	5780 ¹⁵⁴ ₁₄₁	1.24 ^{0.04} _{0.04}
56054	52	6080 ²⁰⁹ ₂₀₉	1.27 ^{0.04} _{0.04}
56056	54	6140 ²²⁷ ₂₀₀	1.27 ^{0.04} _{0.04}
56057	55	6209 ²⁶³ ₂₃₈	1.29 ^{0.04} _{0.04}
56058	56	6280 ²⁴³ ₂₁₁	1.30 ^{0.04} _{0.04}
56059	57	6380 ²⁵³ ₂₂₂	1.31 ^{0.04} _{0.03}
56061	59	6420 ²⁵⁸ ₂₁₈	1.32 ^{0.04} _{0.03}
56062	60	6375 ²⁴⁹ ₂₃₈	1.31 ^{0.04} _{0.05}
56064	62	6420 ²⁴² ₂₂₇	1.32 ^{0.05} _{0.04}
56066	64	6060 ¹⁶⁶ ₁₆₁	1.29 ^{0.05} _{0.04}
56070	68	6000 ¹⁴⁴ ₁₄₆	1.28 ^{0.05} _{0.04}
56072	70	5960 ¹⁶⁴ ₁₅₂	1.26 ^{0.05} _{0.04}
56086	84	5900 ¹⁵¹ ₁₅₈	1.23 ^{0.05} _{0.05}
56087	85	5840 ¹⁵⁴ ₁₄₀	1.21 ^{0.05} _{0.05}
56088	86	5480 ¹⁷² ₁₅₂	1.11 ^{0.06} _{0.05}
56089	87	5480 ¹⁵⁶ ₁₃₉	1.11 ^{0.05} _{0.05}
56097	95	5760 ¹²³ ₁₀₇	1.13 ^{0.05} _{0.05}

Table A1 – *continued* A List of the Temperatures and Bolometric Luminosities

SN2012ec			
56154	11	10020 ³⁴⁵ ₃₂₆	2.26 ^{0.09} _{0.08}
56155	12	9780 ³³² ₃₀₄	2.14 ^{0.08} _{0.07}
56158	15	9068 ⁹²⁶ ₅₃₄	1.85 ^{0.16} _{0.13}
56159	16	8080 ²⁰³ ₁₉₆	1.69 ^{0.04} _{0.04}
56165	22	6880 ¹⁰¹ ₁₀₇	1.44 ^{0.15} _{0.13}
56168	25	6640 ¹⁰¹ ₈₈	1.36 ^{0.14} _{0.12}
56171	28	6480 ⁹² ₁₀₀	1.33 ^{0.13} _{0.10}
56173	30	6620 ¹⁴⁸ ₁₃₄	1.40 ^{0.29} _{0.19}
56176	33	6560 ¹³⁶ ₁₄₂	1.40 ^{0.17} _{0.12}
56179	36	6200 ¹²⁴ ₁₃₂	1.28 ^{0.11} _{0.09}
56181	38	6160 ¹¹⁵ ₁₂₂	1.27 ^{0.15} _{0.12}
56182	39	6120 ¹¹⁰ ₁₂₃	1.26 ^{0.06} _{0.05}
56186	43	6180 ¹²⁵ ₁₂₉	1.30 ^{0.05} _{0.04}
56190	47	6120 ¹²⁷ ₁₀₈	1.28 ^{0.05} _{0.05}
56195	52	6150 ¹⁵² ₁₃₆	1.32 ^{0.06} _{0.06}
56199	56	6220 ¹²⁷ ₁₁₆	1.36 ^{0.04} _{0.04}
56202	59	6099 ¹⁵⁹ ₁₅₁	1.32 ^{0.04} _{0.05}
56204	61	6000 ¹²² ₁₀₃	1.29 ^{0.04} _{0.04}
56208	65	5960 ¹³³ ₁₂₂	1.30 ^{0.04} _{0.03}
56211	68	5840 ¹⁰⁶ ₁₀₄	1.25 ^{0.04} _{0.03}
56212	69	5780 ¹⁰⁷ ₁₂₂	1.24 ^{0.04} _{0.04}
56216	73	5680 ¹¹³ ₁₀₄	1.22 ^{0.05} _{0.05}
SN2013ab			
56344	4	17620 ³³⁰ ₂₉₉	5.54 ^{0.18} _{0.16}
56345	5	15490 ⁵⁹⁶ ₅₃₄	4.73 ^{0.35} _{0.25}
56346	6	14258 ¹⁰⁷³ ₉₁₁	4.15 ^{0.40} _{0.32}
56347	7	12768 ⁵⁷⁰ ₄₉₁	3.66 ^{0.19} _{0.16}
56348	8	11885 ²⁶⁸ ₂₅₄	3.35 ^{0.11} _{0.10}
56349	9	11210 ³²⁶ ₄₀₁	3.07 ^{0.13} _{0.15}
56350	10	10380 ¹⁰⁵ ₁₁₂	2.73 ^{0.04} _{0.04}
56351	11	9996 ²³¹ ₃₈₇	2.54 ^{0.09} _{0.12}
56352	12	9645 ²⁶⁴ ₂₆₆	2.41 ^{0.08} _{0.08}
56353	13	9349 ²⁵⁰ ₂₃₃	2.21 ^{0.10} _{0.09}
56354	14	9040 ¹⁸³ ₁₆₀	2.09 ^{0.04} _{0.04}
56355	15	8928 ⁴⁶⁵ ₂₅₇	2.04 ^{0.13} _{0.06}
56356	16	9080 ²⁸² ₂₈₄	2.04 ^{0.07} _{0.07}
56357	17	8826 ³⁹⁰ ₃₂₉	2.00 ^{0.09} _{0.07}
56358	18	8690 ²⁶⁷ ₂₅₇	1.96 ^{0.06} _{0.06}
56359	19	8620 ²⁶⁸ ₂₄₃	1.94 ^{0.06} _{0.05}
56360	20	8368 ³¹⁵ ₂₈₆	1.87 ^{0.07} _{0.06}
56361	21	8220 ²³³ ₂₂₆	1.83 ^{0.05} _{0.04}
56362	22	7960 ²²⁹ ₂₀₁	1.75 ^{0.04} _{0.04}

Table A1 – *continued* A List of the Temperatures and Bolometric Luminosities

56363	23	7920 ²²³ ₂₀₂	1.74 ^{0.04} _{0.04}
56364	24	7560 ²⁰² ₁₈₂	1.67 ^{0.04} _{0.03}
56365	25	7540 ¹⁹⁵ ₁₈₆	1.65 ^{0.03} _{0.03}
56366	26	7380 ²¹⁵ ₁₉₈	1.57 ^{0.04} _{0.04}
56368	28	7190 ⁵⁶⁰ ₂₀₆	1.51 ^{0.10} _{0.04}
56370	30	7080 ³⁵⁴ ₃₃₅	1.44 ^{0.06} _{0.05}
56372	32	7016 ⁴⁵² ₃₈₀	1.40 ^{0.08} _{0.05}
56373	33	6940 ³⁴⁹ ₃₀₉	1.37 ^{0.05} _{0.04}
56374	34	6800 ³²⁹ ₃₀₃	1.34 ^{0.05} _{0.04}
56376	36	6720 ³²⁷ ₂₉₀	1.31 ^{0.04} _{0.04}
56377	37	6680 ³¹⁴ ₂₉₃	1.29 ^{0.04} _{0.04}
56378	38	6680 ³³³ ₃₀₉	1.28 ^{0.04} _{0.04}
56380	40	6620 ³¹⁵ ₂₈₂	1.26 ^{0.04} _{0.03}
56381	41	6580 ³¹⁵ ₂₇₅	1.25 ^{0.04} _{0.03}
56382	42	6500 ²⁹⁰ ₂₈₁	1.24 ^{0.04} _{0.03}
56383	43	6580 ³¹³ ₂₇₆	1.22 ^{0.04} _{0.03}
56384	44	6650 ³²⁹ ₂₉₄	1.23 ^{0.04} _{0.03}
56388	48	6260 ²⁷⁸ ₂₅₅	1.19 ^{0.03} _{0.03}
56389	49	6220 ²⁸³ ₂₇₄	1.17 ^{0.03} _{0.03}
56390	50	6240 ²⁹³ ₂₆₇	1.15 ^{0.03} _{0.03}
56394	54	6299 ⁴⁰⁸ ₃₂₅	1.14 ^{0.05} _{0.03}
56395	55	6380 ³¹⁹ ₂₇₁	1.15 ^{0.04} _{0.03}
56397	57	6500 ³¹³ ₂₉₉	1.15 ^{0.04} _{0.03}
56398	58	6380 ³⁰³ ₂₈₄	1.13 ^{0.03} _{0.03}
56402	62	6300 ³⁰⁶ ₂₆₇	1.13 ^{0.03} _{0.03}
56403	63	6280 ³⁰⁷ ₂₆₄	1.10 ^{0.03} _{0.03}
56404	64	6380 ³⁰⁸ ₂₈₀	1.14 ^{0.03} _{0.03}
56405	65	6320 ²⁹² ₂₈₃	1.13 ^{0.03} _{0.03}
56406	66	6240 ³⁰⁸ ₂₈₈	1.12 ^{0.03} _{0.03}
56407	67	6220 ²⁹³ ₂₆₄	1.11 ^{0.03} _{0.02}
56409	69	6347 ³⁷⁸ ₃₁₁	1.14 ^{0.04} _{0.03}
56411	71	6300 ²⁹³ ₂₇₈	1.13 ^{0.03} _{0.03}
56412	72	6220 ²⁹⁷ ₂₆₁	1.10 ^{0.03} _{0.03}
56413	73	6180 ³⁰² ₂₅₁	1.07 ^{0.03} _{0.02}
56414	74	6120 ²⁶² ₂₄₆	1.06 ^{0.02} _{0.02}
56415	75	6700 ³⁸¹ ₃₄₄	1.13 ^{0.05} _{0.04}
56416	76	6460 ³⁶² ₃₀₉	1.09 ^{0.04} _{0.03}
56419	79	6140 ²⁸⁶ ₂₅₂	1.05 ^{0.03} _{0.02}
56420	80	6080 ²⁶⁴ ₂₆₀	1.05 ^{0.02} _{0.02}
56421	81	5760 ²⁴⁴ ₂₂₄	1.01 ^{0.02} _{0.02}
56422	82	5960 ²⁵⁹ ₂₄₄	1.02 ^{0.02} _{0.02}
56423	83	5940 ²⁶⁴ ₂₃₇	1.01 ^{0.02} _{0.02}
56426	86	6115 ⁴¹¹ ₃₅₄	0.99 ^{0.04} _{0.03}
56427	87	5800 ²⁵¹ ₂₃₆	0.95 ^{0.02} _{0.02}
56428	88	5760 ²⁵⁶ ₂₁₇	0.94 ^{0.02} _{0.02}

Table A1 – *continued* A List of the Temperatures and Bolometric Luminosities

56429	89	6020 ²⁷² ₂₄₇	0.95 ^{0.02} _{0.02}
56430	90	5860 ²⁵⁵ ₂₂₃	0.92 ^{0.02} _{0.02}
56431	91	5760 ²⁴⁶ ₂₁₅	0.90 ^{0.02} _{0.02}
56432	92	6180 ³³⁰ ₂₈₀	0.90 ^{0.03} _{0.02}
56433	93	5776 ⁶⁴⁶ ₃₉₃	0.86 ^{0.06} _{0.03}
56434	94	5580 ²²⁹ ₂₀₇	0.83 ^{0.02} _{0.02}
56435	95	5663 ⁴⁴⁴ ₃₀₂	0.82 ^{0.02} _{0.02}
56436	96	5900 ²⁹⁹ ₂₅₄	0.81 ^{0.02} _{0.02}
56437	97	5780 ²⁷⁷ ₂₅₀	0.75 ^{0.02} _{0.02}
56438	98	5664 ³⁶⁵ ₃₁₇	0.69 ^{0.03} _{0.03}
56439	99	5760 ²⁷⁶ ₂₄₇	0.66 ^{0.01} _{0.01}
56440	100	5446 ³¹⁸ ₂₈₇	0.62 ^{0.02} _{0.02}
56441	101	5480 ²⁴⁵ ₂₂₄	0.59 ^{0.01} _{0.01}
56442	102	5112 ⁴⁶⁰ ₄₇₇	0.54 ^{0.02} _{0.02}
56443	103	4860 ²⁴⁷ ₂₂₂	0.49 ^{0.02} _{0.02}
56444	104	4865 ⁴⁷⁰ ₃₅₃	0.46 ^{0.02} _{0.02}
56445	105	4840 ²³⁶ ₂₂₇	0.42 ^{0.02} _{0.02}
56446	106	4700 ²³³ ₂₀₄	0.40 ^{0.02} _{0.02}
56448	108	4380 ¹⁵⁹ ₁₃₇	0.37 ^{0.01} _{0.01}
56449	109	4580 ¹⁷⁶ ₁₄₈	0.35 ^{0.01} _{0.01}
56451	111	4500 ¹⁷⁰ ₁₄₃	0.31 ^{0.01} _{0.01}
56454	114	4880 ²³⁷ ₂₃₄	0.27 ^{0.01} _{0.01}
56456	116	4620 ²²⁶ ₁₉₆	0.28 ^{0.01} _{0.01}
56457	117	4840 ¹⁸⁰ ₁₈₁	0.27 ^{0.01} _{0.01}
56458	118	4880 ¹⁹⁴ ₁₇₄	0.26 ^{0.01} _{0.01}
56460	120	4760 ¹⁷³ ₁₇₆	0.25 ^{0.01} _{0.01}
56461	121	5520 ³⁴³ ₂₉₅	0.25 ^{0.01} _{0.01}
56464	124	4808 ²⁴³ ₂₀₈	0.24 ^{0.01} _{0.01}
56466	126	4770 ²⁰² ₁₈₆	0.24 ^{0.01} _{0.01}
56468	128	4460 ²⁰⁹ ₁₉₃	0.26 ^{0.02} _{0.01}
56470	130	4620 ²³⁵ ₁₉₉	0.24 ^{0.01} _{0.01}
56476	136	4480 ²²⁰ ₁₈₇	0.24 ^{0.01} _{0.01}
56477	137	4800 ²⁴² ₂₂₅	0.23 ^{0.01} _{0.01}
56478	138	4980 ²⁵⁶ ₂₄₈	0.21 ^{0.01} _{0.01}
56479	139	4680 ²⁴¹ ₂₀₅	0.22 ^{0.01} _{0.01}
56480	140	4800 ²⁴² ₂₂₅	0.21 ^{0.01} _{0.01}
56481	141	4640 ²²⁵ ₂₁₁	0.22 ^{0.01} _{0.01}
56485	145	5080 ²⁷⁸ ₂₄₈	0.20 ^{0.01} _{0.01}
56487	147	4940 ²⁵⁵ ₂₄₁	0.20 ^{0.01} _{0.01}
56489	149	4840 ²⁸⁷ ₂₅₀	0.19 ^{0.01} _{0.01}
SN2013by			
56407	0	22890 ⁸³³ ₇₈₁	23.65 ^{1.80} _{1.62}
56408	1	19258 ¹⁰⁹⁶ ₇₀₄	18.89 ^{2.62} _{1.74}
56409	2	16860 ⁵⁴⁹ ₅₁₂	16.23 ^{0.99} _{0.88}

Table A1 – *continued* A List of the Temperatures and Bolometric Luminosities

56410	3	14923 ⁷⁰⁴ ₅₅₂	13.53 ^{1.09} _{0.79}
56411	4	13940 ³⁵⁰ ₃₄₃	12.41 ^{0.51} _{0.48}
56412	5	12422 ⁴⁹¹ ₁₁₇₃	10.76 ^{0.65} _{1.36}
56413	6	11304 ⁴⁴⁰ ₃₈₉	9.73 ^{0.51} _{0.43}
56414	7	10875 ⁵⁶² ₄₇₇	9.09 ^{0.70} _{0.48}
56416	9	9991 ⁴⁷⁴ ₄₃₇	8.12 ^{0.34} _{0.32}
56417	10	9500 ²⁸⁹ ₂₇₅	7.47 ^{0.24} _{0.22}
56418	11	9340 ²⁸⁷ ₂₅₃	7.29 ^{0.23} _{0.19}
56419	12	8984 ⁴⁸⁷ ₃₀₉	6.88 ^{0.21} _{0.26}
56423	16	8272 ⁵⁸¹ ₃₃₄	5.54 ^{0.35} _{0.19}
56424	17	8377 ³⁷⁹ ₃₅₉	5.36 ^{0.27} _{0.30}
56426	19	8060 ³²⁴ ₃₀₅	4.88 ^{0.16} _{0.14}
56427	20	7794 ⁷³⁶ ₆₀₇	4.58 ^{0.43} _{0.32}
56428	21	8455 ⁸⁸¹ ₇₂₄	4.91 ^{0.63} _{0.43}
56429	22	8540 ⁸⁹⁵ ₇₄₃	4.89 ^{0.64} _{0.45}
56434	27	7180 ⁶⁰¹ ₅₁₃	3.65 ^{0.25} _{0.18}
56436	29	7010 ⁵⁸⁷ ₄₈₆	3.48 ^{0.23} _{0.16}
56437	30	6880 ⁵⁶³ ₄₅₅	3.38 ^{0.20} _{0.14}
56438	31	7020 ⁵⁷⁴ ₄₈₅	3.38 ^{0.21} _{0.15}
56439	32	6720 ⁵¹⁸ ₄₅₀	3.18 ^{0.16} _{0.12}
56440	33	6700 ⁵²⁰ ₄₃₆	3.18 ^{0.16} _{0.12}
56442	35	6620 ⁵¹¹ ₄₂₂	3.14 ^{0.15} _{0.11}
56444	37	6576 ⁴⁹³ ₄₃₀	3.12 ^{0.14} _{0.11}
56445	38	6640 ⁵⁰⁹ ₄₃₂	2.89 ^{0.14} _{0.10}
56447	40	6478 ⁶⁰² ₅₁₈	2.88 ^{0.13} _{0.12}
56448	41	6720 ⁵⁰⁹ ₄₅₀	2.92 ^{0.15} _{0.11}
56449	42	6305 ⁸⁰⁷ ₆₃₅	2.79 ^{0.20} _{0.14}
56450	43	6180 ⁴⁴² ₃₆₃	2.78 ^{0.09} _{0.08}
56451	44	6520 ⁴⁸⁴ ₄₁₇	2.81 ^{0.12} _{0.09}
56453	46	5900 ³⁸² ₃₄₂	2.50 ^{0.07} _{0.07}
56456	49	5860 ³⁸⁴ ₃₃₂	2.50 ^{0.07} _{0.07}
56458	51	5760 ³⁶⁷ ₃₂₁	2.42 ^{0.07} _{0.06}
56460	53	5660 ³⁶³ ₃₀₂	2.35 ^{0.07} _{0.06}
56462	55	5720 ³⁶⁸ ₃₁₁	2.29 ^{0.06} _{0.06}
56464	57	5780 ³⁷⁵ ₃₂₁	2.23 ^{0.06} _{0.06}
56465	58	5620 ³³⁷ ₃₁₅	2.18 ^{0.06} _{0.06}
56466	59	5480 ³²⁴ ₂₉₄	2.15 ^{0.07} _{0.06}
56468	61	5820 ³⁷⁶ ₃₃₀	2.08 ^{0.06} _{0.06}
56470	63	5880 ³⁷⁷ ₃₄₁	2.03 ^{0.06} _{0.05}
56472	65	5620 ³⁵¹ ₃₀₄	1.95 ^{0.06} _{0.05}
56473	66	5640 ³⁴⁸ ₃₀₉	1.89 ^{0.06} _{0.05}
56474	67	5660 ³⁵³ ₃₁₁	1.81 ^{0.05} _{0.05}
56476	69	5400 ³¹⁹ ₂₈₁	1.70 ^{0.06} _{0.05}
56477	70	5420 ³³⁰ ₂₇₇	1.58 ^{0.05} _{0.05}
56478	71	5380 ³¹⁵ ₂₈₀	1.54 ^{0.05} _{0.05}

Table A1 – *continued* A List of the Temperatures and Bolometric Luminosities

56481	74	5183 ²⁹⁶ ₂₇₈	1.40 ^{0.06} _{0.07}
56482	75	5173 ²⁸⁶ ₂₆₁	1.34 ^{0.05} _{0.05}
56483	76	5188 ²⁹⁴ ₂₅₈	1.26 ^{0.05} _{0.04}
56486	79	5080 ²⁷⁰ ₂₅₅	1.07 ^{0.05} _{0.04}
56487	80	5012 ²⁸² ₂₆₃	1.00 ^{0.05} _{0.05}
56488	81	4816 ²⁵⁵ ₂₃₄	0.88 ^{0.05} _{0.04}
56489	82	5172 ³⁹¹ ₄₃₃	0.76 ^{0.05} _{0.10}
<hr/>			
SN2013ej			
<hr/>			
56500	3	13900 ⁷²⁴ ₈₄₁	4.00 ^{0.33} _{0.28}
56501	4	13053 ⁵³⁷ ₄₈₈	4.02 ^{0.29} _{0.24}
56502	5	12853 ⁷⁴⁹ ₆₆₅	4.33 ^{0.46} _{0.38}
56503	6	11493 ¹¹⁷⁰ ₁₇₃	4.14 ^{0.57} _{0.42}
56504	7	11488 ⁷⁵⁷ ₅₅₉	4.19 ^{0.40} _{0.34}
56505	8	11271 ⁶⁴⁶ ₄₀₇	4.08 ^{0.60} _{0.37}
56506	9	11145 ⁶²⁵ ₆₂₅	4.28 ^{0.36} _{0.29}
56507	10	10489 ⁵³⁴ ₄₅₀	4.07 ^{0.32} _{0.24}
56508	11	10452 ⁵⁴⁵ ₅₃₉	4.07 ^{0.31} _{0.26}
56509	12	10220 ⁴⁸⁰ ₄₃₃	4.02 ^{0.28} _{0.23}
56510	13	10018 ¹²²⁴ ₆₆₆	3.92 ^{0.86} _{0.35}
56511	14	10600 ¹³⁰² ₉₉₅	4.41 ^{0.99} _{0.64}
56512	15	10560 ¹²⁸⁸ ₉₉₆	4.43 ^{0.98} _{0.64}
56513	16	10339 ¹⁴⁴⁸ ₁₁₂₁	4.25 ^{1.16} _{0.74}
56514	17	10183 ¹⁵²⁵ ₉₇₂	4.20 ^{1.12} _{0.59}
56515	18	9856 ¹²⁷⁷ ₁₀₄₃	3.91 ^{0.88} _{0.57}
56516	19	9410 ⁸⁴⁸ ₇₀₉	3.67 ^{0.51} _{0.38}
56520	23	9580 ¹⁵¹⁶ ₁₁₀₈	3.83 ^{1.05} _{0.62}
56521	24	9784 ¹⁵³⁶ ₁₁₂₅	3.95 ^{1.13} _{0.69}
56522	25	9775 ¹⁵⁵⁸ ₁₁₄₂	3.84 ^{1.11} _{0.65}
56524	27	8975 ¹⁵⁴⁷ ₉₇₉	3.22 ^{0.93} _{0.46}
56525	28	9054 ¹³⁶⁸ ₁₁₈₇	3.29 ^{0.82} _{0.56}
56526	29	8620 ¹¹³⁸ ₈₅₅	3.03 ^{0.61} _{0.38}
56528	31	8640 ¹¹⁴⁴ ₈₆₀	2.93 ^{0.59} _{0.37}
56529	32	8737 ¹¹⁵⁴ ₈₉₆	2.93 ^{0.60} _{0.40}
56533	36	8180 ¹⁰⁰⁶ ₇₉₁	2.50 ^{0.43} _{0.28}
56534	37	8060 ¹⁰⁰⁴ ₇₈₁	2.42 ^{0.41} _{0.26}
56538	41	7040 ¹³⁵⁹ ₉₆₂	1.91 ^{0.43} _{0.21}
56539	42	7560 ¹³⁹⁴ ₁₀₀₀	2.02 ^{0.51} _{0.27}
56541	44	7520 ¹³⁶³ ₉₉₇	1.92 ^{0.47} _{0.25}
56544	47	7400 ¹³⁰¹ ₉₇₁	1.84 ^{0.42} _{0.23}
56546	49	6920 ¹¹⁵⁷ ₈₄₀	1.65 ^{0.31} _{0.16}
56553	56	6520 ⁹⁶⁸ ₇₅₇	1.48 ^{0.21} _{0.12}
56554	57	6940 ¹¹²⁴ ₈₅₃	1.53 ^{0.28} _{0.16}
56560	63	6580 ¹⁰²³ ₇₅₁	1.35 ^{0.21} _{0.11}
56562	65	6520 ⁹⁶⁸ ₇₅₇	1.35 ^{0.19} _{0.11}

Table A1 – *continued* A List of the Temperatures and Bolometric Luminosities

56563	66	6800^{1097}_{805}	$1.34^{0.24}_{0.12}$
56567	70	6440^{953}_{732}	$1.25^{0.17}_{0.09}$
56568	71	6340^{915}_{713}	$1.21^{0.16}_{0.09}$
56573	76	6600^{1003}_{771}	$1.16^{0.18}_{0.10}$
56574	77	6800^{1097}_{805}	$1.16^{0.21}_{0.11}$
56577	80	6920^{1125}_{843}	$1.14^{0.21}_{0.11}$
56578	81	6540^{981}_{758}	$1.05^{0.15}_{0.09}$
56589	92	6700^{1056}_{784}	$0.79^{0.13}_{0.07}$
56594	97	6560^{993}_{759}	$0.59^{0.09}_{0.05}$
56596	99	5980^{812}_{630}	$0.44^{0.04}_{0.02}$
56600	103	6420^{1135}_{837}	$0.22^{0.04}_{0.02}$
56607	110	6180^{1358}_{933}	$0.15^{0.03}_{0.01}$
56610	113	6980^{2924}_{1539}	$0.16^{0.09}_{0.02}$
56613	116	5960^{1815}_{1111}	$0.12^{0.03}_{0.01}$
56616	119	6440^{1638}_{1072}	$0.13^{0.03}_{0.01}$
56617	120	5960^{1722}_{1075}	$0.13^{0.03}_{0.01}$